Catena 212 (2022) 106110

Contents lists available at ScienceDirect

Catena

journal homepage: www.elsevier.com/locate/catena

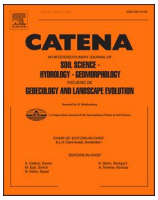

Factors influencing the ground thermal regime in a mid-latitude glacial cirque (Hoyo Empedrado, Cantabrian Mountains, 2006–2020)

Adrián Melón-Nava *, Javier Santos-González, José María Redondo-Vega, Rosa Blanca González-Gutiérrez, Amelia Gómez-Villar

Department of Geography and Geology, Universidad de León, León 24071, Spain

ARTICLE INFO

Keywords:
Ground thermal regime
Mountain permafrost
Talus slope
Rock glacier
Air convection
Cantabrian Mountains

ABSTRACT

Air and near-surface ground temperatures were measured using dataloggers over 14 years (2006–2020) in 10 locations at 2262 to 2471 m.a.s.l. in a glacial cirque of the Cantabrian Mountains. These sites exhibit relevant differences in terms of substrate, solar radiation, orientation, and geomorphology. Basal temperature of snow (BTS) measurements and electrical resistivity tomography of the talus slope were also performed. The mean annual near-surface ground temperatures ranged from 5.1 °C on the sunny slope to 0.2 °C in the rock glacier furrow, while the mean annual air temperature was 2.5 °C. Snow cover was inferred from near-surface ground temperature (GST) data, estimating between 130 and 275 days per year and 0.5 to 7.1 m snow thickness. Temperature and BTS data show that the lowest part of the talus slope and the rock glacier furrow are the coldest places in this cirque, coinciding with a more persistent and thickest snow cover. The highest temperatures coincide with less snow cover, fine-grained soils, and higher solar radiation. Snow cover has a primary role in controlling GST, as the delayed appearance in autumn or delayed disappearance in spring have a cooling effect, but no correlation with mean annual near-surface ground temperatures exists. Heavy rain-over-snow events have an important influence on the GST. In the talus slope, air circulation during the snow-covered period produces a cooling effect in the lower part, especially during the summer. Significant inter-annual GST differences were observed that exhibited BTS limitations. A slight positive temperature trend was detected but without statistically significance and less prominent than nearby reference official meteorological stations, so topoclimatic conditions reduced the more global positive temperature trend. Probable existence of permafrost in the rock glacier furrow and the lowest part of the talus slope is claimed; however, future work is necessary to confirm this aspect.

1. Introduction

The ground thermal regime is a significant issue in geomorphology because it is the main parameter influencing geomorphological processes in periglacial mountain regions (Serrano et al., 2020; Vieira et al., 2003). Some countries have established long-term monitoring of ground temperature data (Streletskiy et al., 2015); however, in mid-latitude mountainous areas, data are scarce and frequently cover only 1–2 y, with some exceptions (Bodin et al., 2009; Kellerer-Pirklbauer, 2019; Morard et al., 2010; Staub et al., 2015).

Meteorology, terrain, and subsurface characteristics are primary influencing factors on near-surface ground temperatures (GST); however, seasonal snow cover is regarded as the second most important influence (Williams and Gold, 1976). Mainly due to the influence of snow cover, the air and ground temperatures are not well correlated in artic and alpine areas (Thorn et al., 1999); hence, it is necessary to obtain direct records of ground temperatures with sensors. Miniature temperature data loggers are widely used for this purpose (Hoelzle et al., 1999). Snow cover is a key factor influencing GST (Ferreira et al., 2017; Hrbáček et al., 2020; Ishikawa, 2003; Luetschg et al., 2008; Rödder and Kneisel, 2012; Zhang, 2005; Zhao et al., 2018), lowering the mean annual ground temperature (MAGST) with respect to mean annual air temperature (MAAT) in some locations but also increasing the average in cold climate environments (Davesne et al., 2017). Thermal isolation of snow occurs mainly at a thickness of 40–60 cm (Hanson and Hoelzle, 2004; Luetschg et al., 2008; Zhang, 2005); however, a thin (<20 cm) snow cover also have a high transcendence by cooling the ground (Davesne et al., 2017; Zhao et al., 2018; Zhou et al., 2013). In fact, some

* Corresponding author.
E-mail address: amelon@unileon.es (A. Melón-Nava).

https://doi.org/10.1016/j.catena.2022.106110
Received 28 March 2021; Received in revised form 19 November 2021; Accepted 1 February 2022
Available online 15 February 2022

authors (Harris et al., 2009) consider snow distribution an important variable that determines permafrost temperature. Snow also acts as a primary agent controlling periglacial dynamics and landforms (Gómez-Ortiz et al., 2019; Pellitero et al., 2019; Pisabarro et al., 2017; Serrano et al., 2020).

The role of other factors in thermal behaviour has been analysed in several studies, including as one of the most relevant substrate influences. Different studies in mountainous areas (Harris and Pedersen, 1998; Juliussen and Humlum, 2008; Onaca et al., 2020; Rödder and Kneisel, 2012; Schneider et al., 2012) as well as in the laboratory (Yu et al., 2004) have shown colder temperatures in blocky materials than in adjacent terrains. In these boulders' deposits, including talus slopes and rock glaciers, air convection has been observed, generating relevant temperature differences between the lower part of the deposits, where dense cold air is accumulated, and the upper one, which show higher values. This air exchange has been explained by processes such as the chimney effect (Delaloye and Lambiel, 2005; Popescu et al., 2017; Sawada et al., 2003; Wakonigg, 1996). This process explains the location of permafrost well below its regional limit in favourable topographic locations (Kellerer-Pirklbauer, 2019; Kneisel et al., 2000; Onaca et al., 2015; Popescu et al., 2017; Stiegler et al., 2014).

The complex mountainous terrain shows great variability in terms of topography, snow conditions, temperatures, or solar radiation (i.e. Thorn et al., 1999; Sawada, Ishikawa and Ono, 2003; Rödder and Kneisel, 2012); therefore, monitoring different environments is essential for obtaining a complete view of GST. Glacial cirques are widespread landforms in many mid-latitude mountain ranges, showing a distinctive morphology with relatively low variations (Evans and Cox, 2015). These landforms show contrasting topography (steep and low-gradient slopes), orientation (and consequently insolation), and some altitudinal range. They are often covered by post-glacial deposits, such as rock glaciers and talus slopes. This generates a mosaic of different environments that are quite similar from one cirque to another. Because of this, glacial cirques are adequate landforms for performing GST analysis and show the possibility of extrapolating the results to similar landforms in analogous climate environments.

In the mid-latitude mountains, climate conditions (including snow cover) vary significantly each year (López-Moreno et al., 2020; Vieira et al., 2003), and a complex ground thermal regime occurs. Therefore, a year of GST data would not be sufficient to obtain a clear view of the thermal behaviour. In the Iberian Peninsula, some ground temperature data have been presented in the Sierra Nevada (Gómez-Ortiz et al., 2011), the Pyrenees (González-García et al., 2017; Serrano et al., 2019), Serra da Estrela (Vieira et al., 2003), and Cantabrian Mountains (Pisabarro, 2020; Pisabarro et al., 2015, 2017; Ruiz-Fernández et al., 2017; Santos-González et al., 2009; Serrano et al., 2020). However, ground temperature variability is still poorly understood, and there is a gap in the long-term monitoring of high mountain environments.

A 14 years record of air temperature (AT) and GST data from nine sites in the Hoyo Empedrado Cirque are presented in this work. The data collected ranged from 2262 to 2471 m.a.s.l. and covered different locations (talus slope, rock glacier furrow and ridge, sunny slope, and summit), different substrates (coarse deposits and fine-grained soils), and places with high variances in insolation data and snow cover duration. The main objectives of this study are as follows:

a) To show spatial differences in ground temperature data.
b) To determine which factors influence those differences.
c) To describe inter-annual differences and evolution, in relation to controlling factors.
d) To evaluate the occurrence of air circulation in a talus slope.
e) To discuss the possible existence of permafrost below its regional limits in the Cantabrian Mountains.

2. Study area

The study area is located in the Peña Prieta massif, in the central part of the Cantabrian Mountains, NW Iberian Peninsula (Fig. 1a). This range is approximately 500 km long and 80 to 120 km wide, between the Cantabrian Sea in the north and the Douro basin in the south (Fig. 1b). The cryosphere in the Cantabrian Mountains is mainly snow cover, seasonal freeze ground, and, to a lesser extent, ice patches and ice caves (Pisabarro et al., 2017).

The Peña Prieta massif is the second highest massif of the range (Peña Prieta, 2539 m.a.s.l.), after Picos de Europa (Torrecerredo, 2648 m.a.s.l.). The study includes one glacial cirque formed on the northern slope of Agujas de Cardaño (2388 m.a.s.l.) and the southwestern slope of Tres Provincias (2499 m.a.s.l.) (Fig. 1c), which is also the headwater of the Lechada valley (Douro River Basin). The lowest altitude of the study area is 2230 m.a.s.l., at the bottom of the cirque. Geologically, the area is a part of the Fuentes Carrionas mantle as well as the Cantabrian Zone which is one of the great units of the Iberian Variscan orogen (Martínez-Catalán et al. 2009). The faults have O-E and SO-NE directions. The cirques are composed of an intrusive body of biotite granodiorites, surrounded by dikes of varied lithological composition (Martín-González and Heredia, 2011; Rodríguez-Fernández et al., 1994).

Glacial landforms are widespread in this massif (Frochoso and Castañón, 1996; Pellitero, 2014, 2022; Pisabarro Pérez et al., 2015; Redondo-Vega and Santos-González, 2013; Santos-González et al., 2022; Serrano et al., 2013). The Local Last Glacial Maximum has been dated in this area in 36 ka BP, when the Lechada valley was occupied by a glacier tongue 8.2 km long, ~200 m thick that reached 1350 m (Pellitero et al., 2019). The equilibrium line altitude estimated using Area-Altitude Balance Ratio method was located at ~ 1880 m, a higher position than other Cantabrian Mountain paleo-glaciers (Santos-González et al., 2013). Some moraines evidence the general trend of deglaciation (Serrano et al., 2015). During the Younger Dryas or the Bølling-Allerød interstadial (Pellitero, 2022), paraglacial/periglacial conditions favoured the formation of two small rock glaciers or protalus lobes (Fig. 1c) (Gómez-Villar et al., 2011; Pellitero et al., 2011; Redondo Vega et al., 2011) in the Hoyo Empedrado Cirque (Serrano et al., 2015). During the Little Ice Age (LIA), some glaciers probably developed in this massif (Prado, 1852). In the Hoyo Empedrado, perennial or semi-perennial snow patches were probably developed. Periglacial landforms are also widespread (screes, terraces, or gelifluxion lobes) (Fig. 1c), with a likely higher activity during the LIA than at present.

The Hoyo Empedrado Cirque is 610 m long, 750 m wide, and 270 m deep. The south-facing slope (Fig. 1h) is composed of Carboniferous sandstones and shales with granodiorite outcrops. The average slope is 27.8° (Fig. 1e), and many gelifluction lobes appear up to 10 m long (Fig. 1c). The north-facing slope is composed of granodiorite, generating a 60 m high vertical rock wall and a talus slope composed of small pebbles and boulders in the upper part and very large (up to 4 m) boulders in the cirque bottom, where two small fossil or inactive creeping landforms appear (Fig. 1g). The highest one is a small talus rock glacier (or protalus lobe according to González-García et al., 2017) that is 79 m long and 128 m wide and consists of a furrow and ridge (Fig. 1c). The other is larger: 85 m long and 151 m wide. This contrasting topography generates relevant differences in potential solar radiation, varying from 7,699 WH/m^2 on the cirque headwalls to 1,713,980 WH/m^2 on the sunny slope (Fig. 1d).

The climate of this area is oceanic and influenced by the high altitude, with moderate Mediterranean influence (i.e. reduced summer precipitation). The annual mean temperature is estimated to be 3.5 °C to 5 °C, and the annual precipitation is greater than 1400 mm (Ortega-Villazán and Morales-Rodríguez, 2015). The snow cover varies greatly depending on the orientation and topography, but persists until July or August in some favourable locations.

Vegetation cover is discontinuous owing to the high altitude and geomorphological processes. It is composed of herbaceous and bush

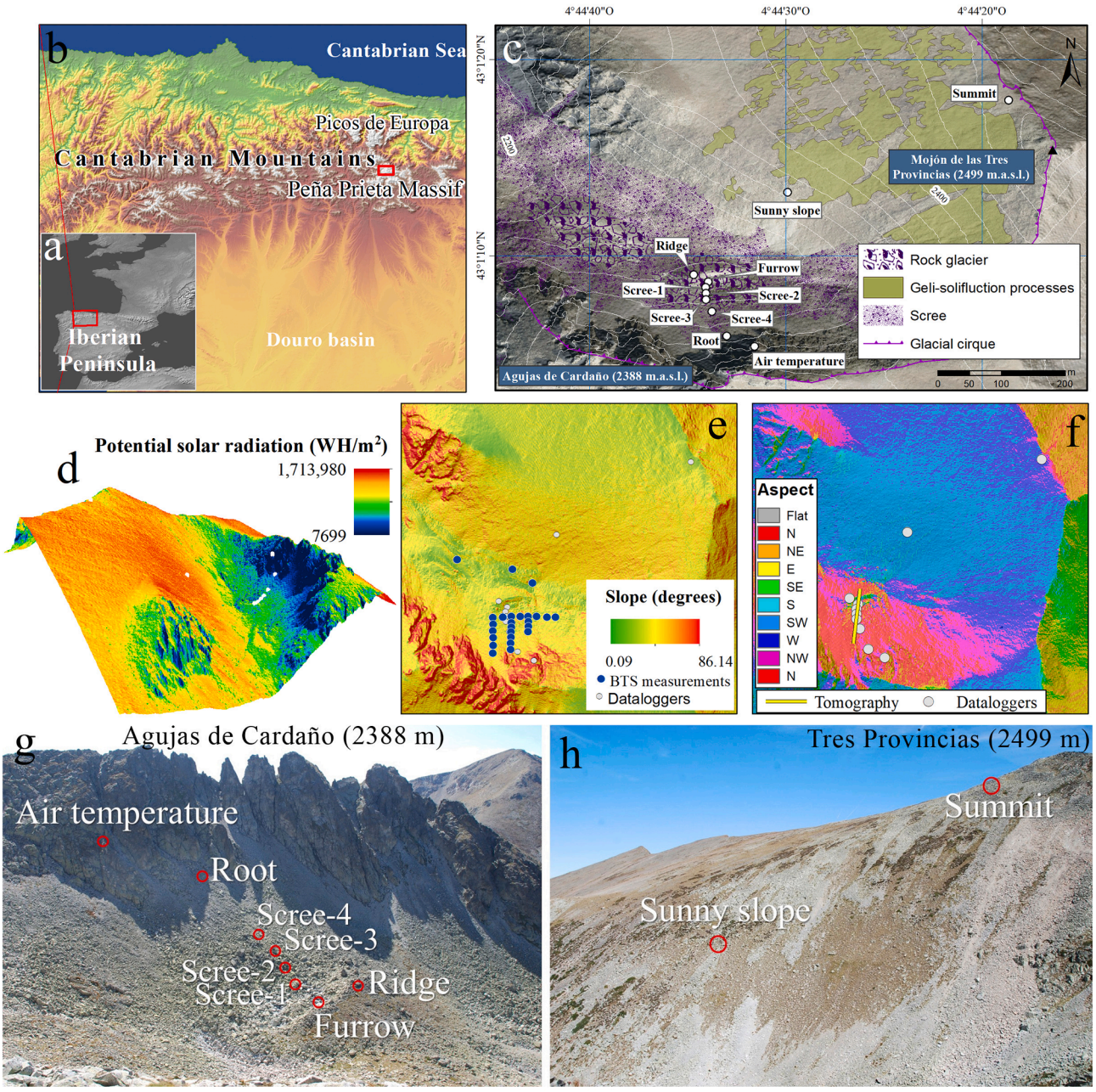

Fig. 1. Study area. a) Location of the study area in southwestern Europe. b) Location of the study area in Cantabrian Mountains. c) Location of dataloggers in the Hoyo Empedrado Cirque and geomorphological map. d) 3D representation of the annual values of potential solar radiation. e) Slope map of the study area showing location of basal temperature of snow measurements. f) Aspect map of the study area showing the position of the electrical resistivity tomography. g) Placement of dataloggers in the north-facing slope. h) Dataloggers in the south-facing slope.

vegetation. At higher altitudes, some shrubs grow, such as common juniper (*Junniperus alpina)* or some Vaccinium species (*Vaccinium myrtillus* and *Vaccinium uliginosum)*. In addition, some species of Fescue emerge (*Festuca indigesta, Festuca lemanii,* and *Festuca eskia*). Alpine ferns (*Cryptogramma crispa*) and herbaceous perennials (*Alchemilla saxatilis*) are found on rock glaciers and talus slopes. It is important to note the presence of endemic flora, such as *Androsace cantabrica*, favoured by a particular soil and climatic conditions.

The study area is part of the 'Montaña de Riaño y Mampodre' Regional Park, and it is also included in the list of sites of community importance and special protection areas of the European Commission Habitats Directive (92/43/EEC).

3. Methods

3.1. Data acquisition and processing

Temperature data were obtained using HOBOware dataloggers. H08-030–08 (HOBO Pro Series) has an operating range from −30 °C to + 50 °C. U23-004 (HOBO U23 Pro v2 External Temperature) operating from −40 °C to 100 °C and achieves an accuracy of ± 0.21 °C from 0 °C to 50 °C and ± 0.25 °C at −10 °C. The data loggers (Table 1) saved hourly records from almost 14 years, from November 2006 to September 2020 in a discontinuous manner (Fig. 2). They were placed below the surficial deposits, varying from fine to very large boulders (Fig. 1g, h).

AT was measured using the same type of dataloggers installed in a steep granodiorite rockwall, where no snow accumulation occurred.

Table 1
Datalogger specifications and geomorphological context.

Datalogger	Elevation (m. a.s.l.)	Aspect	Landform	Type of deposits
Air	2340	North	Rock scarp	–
Root	2315	North	Talus slope (highest part)	Pebble
Scree 4	2288	North	Talus slope (upper part)	Boulders
Scree 3	2277	North	Talus slope (middle part)	Boulders
Scree 2	2271	North	Talus slope (lower part)	Big boulders
Scree 1	2266	North	Talus slope (lowest part)	Very big boulders
Furrow	2262	North	Rock glacier (talus slope base)	Very big boulders
Ridge	2269	Northwest	Rock glacier	Cobbles and sand
Sunny slope	2325	Southwest	Regularized slope	Cobbles and sand
Summit	2471	West	Blockfield border	Gravel and fines

Owing to the presence of some data gaps, the time series was filled by applying a simple linear regression with nearby stations with similar characteristics from the Global Change Monitoring Programme in National Parks of the Spanish Ministry for the Ecological Transition and the Demographic Challenge (http://www.miteco.gob.es/es/red-parques-nacionales/red-seguimiento/). The registered data show a very high correlation with some stations located in Picos de Europa. The greatest correlation ($R^2 = 0.89$) occurred with daily means of Cabaña Verónica meteorological station, located 19 km to the north at 2239 m.a.s.l. In addition, data from Mirador del Cable (situated at 1919 m.a.s.l. and 16 km away) and Coriscao (1750 m.a.s.l. and 9 km away) had acceptable values of correlation ($R^2 = 0.74$ and $R^2 = 0.73$, respectively). Data gaps were filled using the monthly correlation formula from the stations with higher correlation for each month. Monthly correction factors were applied because of the altitude mismatch. They were calculated considering monthly gradients, obtained by altitude, and the monthly mean temperature regression analysis of the four locations. It indicates R^2 values > 0.95, from October to March, and a mean $R^2 = 0.79$, from April to September.

Temperature data were processed using HOBOware software, and statistical analysis was performed using SPSS and R-4.0.3. to calculate:

- Daily maximum, minimum, and arithmetic mean of temperatures (0–24 h).
- Monthly mean, maximum and minimum temperatures.
- Annual mean temperatures, using hydrological year (October-September).
- Monthly freeze–thaw cycles at each datalogger location. Freeze-thaw cycles were calculated considering days when the daily minimum temperature was below −0.2 °C and the daily maximum temperature was above 0.2 °C to rule out erroneous values related to datalogger accuracy (0.2 °C).
- Time series analysis. MAGST and MAAT were evaluated as linear trend-line models and Mann-Kendall statistical test was applied to find significant trends.

In order to display the relationships between variables, correlograms were performed (Supplementary data 1). They refer to temperature and snow attributes, being grouped by hydrological years for each location. Pearson correlation method was applied in R using years with complete observations.

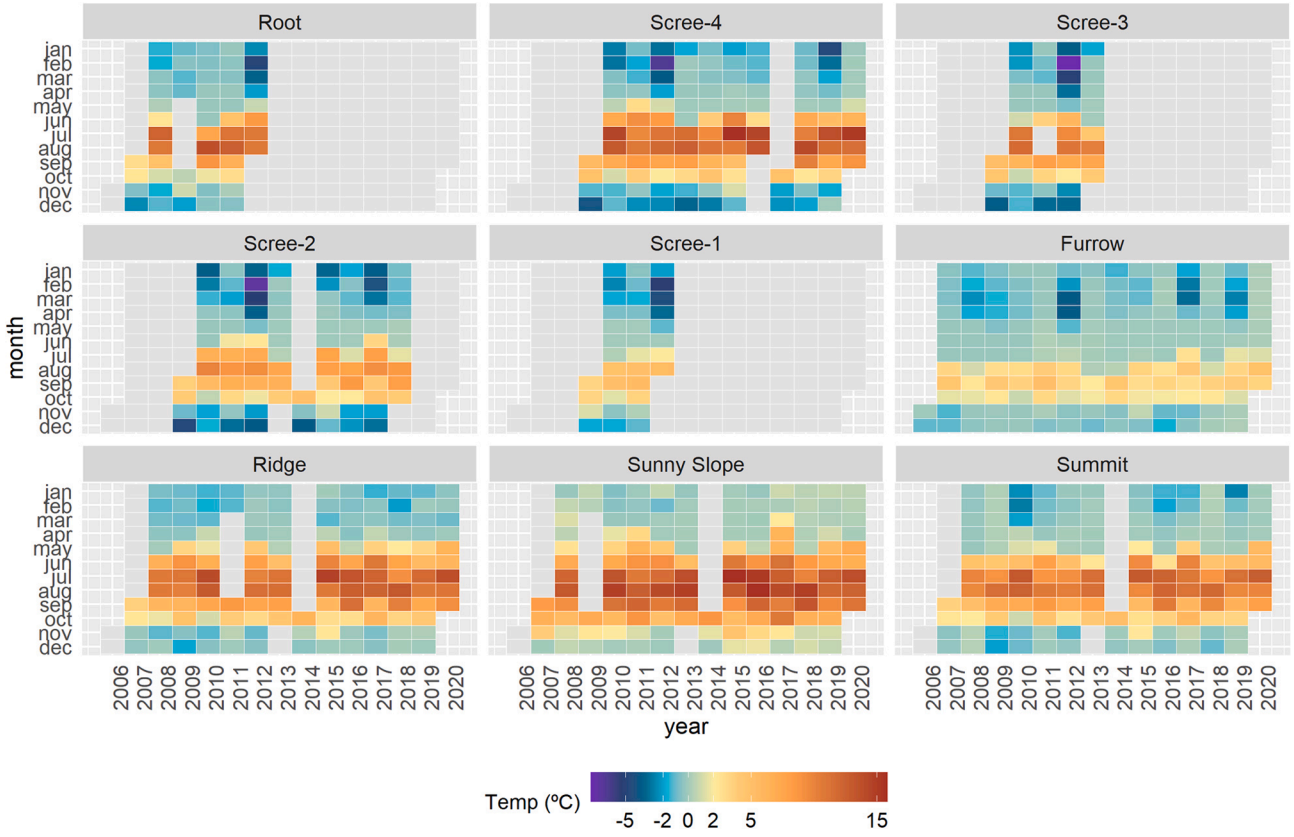

Fig. 2. Heatmap of monthly mean temperatures in the Hoyo Empedrado dataloggers.

3.2. Snow cover data inferred from GST

GST data were used to estimate the snow-covered days (SCD) at each location. The presence and absence of snow as well as the start and end of the melting period in spring has been successfully derived from GST time series (Apaloo et al., 2012; Hoelzle et al., 1999; Schmid et al., 2012). In this case, it was calculated through mean diary temperatures (threshold values of < 1 °C, because it was checked by remote sensing, field work and previous work (Santos-González et al., 2009) that some locations kept temperatures between 0 °C and 1 °C while staying under the snow cover) and daily temperature amplitude (threshold values of $<$ 0.5 °C). The first and last days of isolating the snow cover were manually estimated using GST data.

GST has been used to estimate maximum snow depth. For this purpose, we used the melt index equation developed by Staub and Delaloye (2017): $meltindex[SWE, mm] \cong \frac{\Delta hs \cdot \rho}{\Delta t} \cong \frac{A \cdot \sum_{t=RD}^{SDD} AirT^{+}}{\Delta t_{(SDD-RD)}}$, where:

- SWE is the Snow Water Equivalent (in mm).
- *hs* is snow depth estimated by solving the equation.
- ρ is the snow density. A medium value of 400 kg/m^3 was used. Any snow density measurements were performed in the study area, but snow density data of the Valdecebollas telenivometer, located at 1910 m.a.s.l. and 30 km to the east, was used as a reference (Alonso-González et al., 2018, 2020; Navarro-Serrano and López-Moreno, 2017). In any case, spatial and temporal differences might exist; therefore, this value is only a reference (a density value of 500 kg/m^3 decreases the snow depth by 20%, and a value of 300 kg/m^3 increases snow depth by 33%).
- *t* is the number of days
- *A* is the degree-day factor. We used the value 4.5, as proposed by Zingg (1951) for the Alps and used by Staub and Delaloye (2017). This is a reference value that has not been calibrated in the study area.
- *SDD* is the snow disappearance date, estimated using GST data at each location (first day with positive GST after spring zero curtain).
- *RD* is the start of the spring zero curtain effect (Outcalt et al., 1990), calculated by observing temperature data when the temperature is stable around 0 °C (±0.2 °C).
- T^{+} is the sum of positive mean daily air temperatures during the spring zero curtain effect.

This approach assumes that snow melt is converted in water depending mainly on positive AT during the melting period (Staub and Delaloye, 2017), which coincides with the zero-curtain effect period. However, rain and solar radiation influence melting rates, and both factors are not included in the formula. Among these, other uncertainty exists owing to the lack of monitoring data. For these reasons, snow depth has only been used as a reference and to compare snow accumulations between different locations.

3.3. Digital elevation models, basal temperature of snow, and electrical resistivity tomography

A 1 m digital elevation model (DEM) was developed in the Cloud Compare software using 2012 LiDAR data available in the National Centre for Geographic Information of Spain (IGN/CNIG). The DEM has been used to generate a hillshade and calculate elevation, aspect, slope, and potential solar radiation using ArcMap 10.6.1. Daily mean temperatures were interpolated by inverse distance weighted (IDW) interpolation in ArcMap to generate maps of an estimated evolution of temperatures in the study area.

On 3 April 2009, 25 basal temperature of snow measurements were taken using a 2 m long temperature probe, coupled with a K-thermocouple thermometer (HI 93530) with a resolution of 0.1 °C and accuracy of ± 2% of full scale. The measurement points were separated 15 m from each other by tracing a line perpendicular to the slope in the lower part of the scree and three parallel lines to the slope in the scree, covering the talus slope monitoring sites and the adjacent area (Fig. 1e). Three points were located at the lowest part of the sunny slope. In the lowest part of the talus slope, snow cover was over 3 m, and no measurements could be obtained.

On 13 September 2019, we conducted a 115 m long 2D geoelectrical profile in the Hoyo Empedrado rock glacier with 24 channels and Wenner-Schlumberger measure configuration. A SYSCAL IRIS R1 + 48 channels resistivity meter was used. Then, 24 electrodes were arranged with a separation between the electrodes of 5 m. The existence of large boulders made it difficult to transmit a current in the surface layer, resulting in unstable contact resistances as there are different points of contact between boulders. To compensate for this, large electrodes with attached water-soaked sponges were used to improve the passage of current from the cable to the ground unit. The air temperature was 10 °C, which was considered for data processing. The field data from the tomography were corrected using Prosys II software. The post-processing data were analysed using specific software (RES2DINV version 36.56.06).

Electrical tomography has been usually used to detect mountain permafrost in high mountain environments (Colucci et al., 2019; Duvillard et al., 2018; Emmert and Kneisel, 2017; Hilbich et al., 2009; Mollaret et al., 2019; Ribolini et al., 2010; Scapozza et al., 2011) and the detailed methodology could be found in these works. The diverse resistivity of materials to the electric wave allows us to infer differences in the substrate; thus, it is possible to obtain a vertical profile and determine the internal structure of landforms.

4. Results

4.1. Spatial and interannual variations in air and ground temperatures

The MAAT in the study area during the monitoring period was 2.5 °C (varying between 0.8 °C and 4.0 °C) (Table 2). The mean monthly air temperature ranged from −4.5 °C in February to 10.8 °C in August (Fig. 2). Extreme temperatures were −15.5 °C (04 February 2012 during a very cold period) and 27.0 °C (21 August 2017 during a heatwave). The mean diurnal thermal oscillation was as low as 3.7 °C (2.1 °C in February and 5.3 °C in July) due to the lack of thermal inversion in this summit area. Maximum daily temperatures in winter months were usually below 0 °C; however, higher values were observed in all months (mean of 5 days with positive maximum temperature in February, 9 days in January).

GST exhibited a similar trend evolution to that of AT, with lower temperatures in winter (December to March, depending on location) and higher temperatures in summer (July to September) (Fig. 2, Table 2). GST was higher than AT during the winter months (November to March) but higher or lower than AT depending on location throughout the remainder of the year. Snow cover decoupled AT and GST during most of the year; however, its presence varied depending on location and year and could be present from late October to late August.

Notable differences in MAGST were observed in the study area (Fig. 2, Table 2). The furrow of the rock glacier and the lowest part of the scree had the lowest values. In the furrow, MAGST was 0.3 °C, being negative in 2007–2008 (−0.4 °C), 2011–2012 (−0.2 °C), and 2016–2017 (−0.1 °C) hydrological years. Scree 1 (the lowest part of the talus slope) had the same MAGST (0.3 °C) and −0.5 °C in 2011–2012. Temperature in the talus slope increased towards the upper part (Scree 2 1.0 °C, Scree 3 1.7 °C, Scree 4 2.8 °C, and Root 2.4 °C). The data logger located on the sunny slope had the highest MAGST (5.0 °C). Ridge (3.4 °C) and Summit (3.1 °C) also showed higher values than the talus slope.

The 8- to 14-years temperature series showed a slight increase in AT and GST trend evolution (Fig. 3). Mean temperature tends to increase by ~ 0.04 °C per year in AT and ~ 0.03 °C in Furrow, Scree 2, and in the

Table 2
Mean monthly and annual GST (in °C) in each location, snow cover thickness, and duration. Note that recording periods are heterogeneous in each location and data gaps can be seen in Fig. 3. MAGST (Mean Annual near-Surface Ground Temperature). MMAGST (maximum MAGST). mMAGST (minimum MAGST). MMTO (Mean monthly thermal oscillation). F days (days with negative maximum temperature). F/T days (days with freeze–thaw cycles). T days (Days with positive minimum temperature). SCD (Snow-covered days). MMST (Mean Maximum Snow Thickness, in meters).

Air temperatures		Ground surface temperatures									
			Talus slope					Rock glacier			
	Air		Root	Scree 4	Scree 3	Scree 2	Scree 1	Furrow	Ridge	Sunny slope	Summit
January	-3.5	January	-1.2	-1.9	-2.0	-2.3	-1.5	-0.6	-0.8	0.2	-0.8
February	-4.5	February	-1.6	-1.9	-2.8	-2.4	-3.0	-0.9	-0.7	0.1	-0.7
March	-2.8	March	-1.2	-1.1	-1.7	-1.8	-2.6	-1.2	-0.7	0.5	-0.3
April	0.8	April	-0.7	-0.3	-0.9	-0.8	-1.6	-0.9	0.0	1.2	0.0
May	4.2	May	0.2	0.7	-0.3	-0.1	-0.4	-0.2	2.7	3.4	1.2
June	7.7	June	3.9	6.0	2.6	0.9	0.0	0.0	7.5	8.1	5.6
July	10.4	July	10.5	12.5	8.3	4.9	1.3	0.4	11.6	12.8	10.9
August	10.8	August	12.0	12.2	11.0	8.6	5.1	2.6	11.5	13.9	10.9
September	7.4	September	6.3	7.4	7.0	5.9	5.0	3.5	7.3	10.6	6.9
October	3.6	October	2.0	3.5	2.9	2.9	2.8	2.0	3.5	6.9	3.3
November	-1.6	November	-0.3	-0.9	-1.2	-1.0	0.4	-0.3	-0.1	2.1	-0.1
December	-2.8	December	-1.3	-2.0	-2.9	-2.9	-1.5	-0.5	-0.4	0.6	-0.4
Mean	**2.5**	**MAGST**	**2.4**	**2.8**	**1.7**	**1.0**	**0.3**	**0.3**	**3.4**	**5.0**	**3.1**
Mean Max.	4.0	MMAGST	2.8	3.4	2.1	1.2	0.5	0.9	4.2	6.3	3.6
Mean Min.	0.8	mMAGST	1.9	2.2	0.4	0.4	-0.5	-0.4	2.4	4.3	2.5
MMTO	15.3	MMTO	13.6	14.5	13.9	11.5	8.1	4.7	12.4	13.8	11.7
F days	134	F days	230	197	212	227	237	222	164	62	154
F/T days	56	F/T days	17	19	23	12	10	14	43	20	19
T days	175	T days	118	149	130	126	119	129	158	283	192
-5°C 0°C 5°C 10°C 15°C		SCD	230	188	205	226	239	275	164	134	198
		MMST	3.2	2.0	3.6	4.4	5.6	7.1	0.5	0.9	2.1

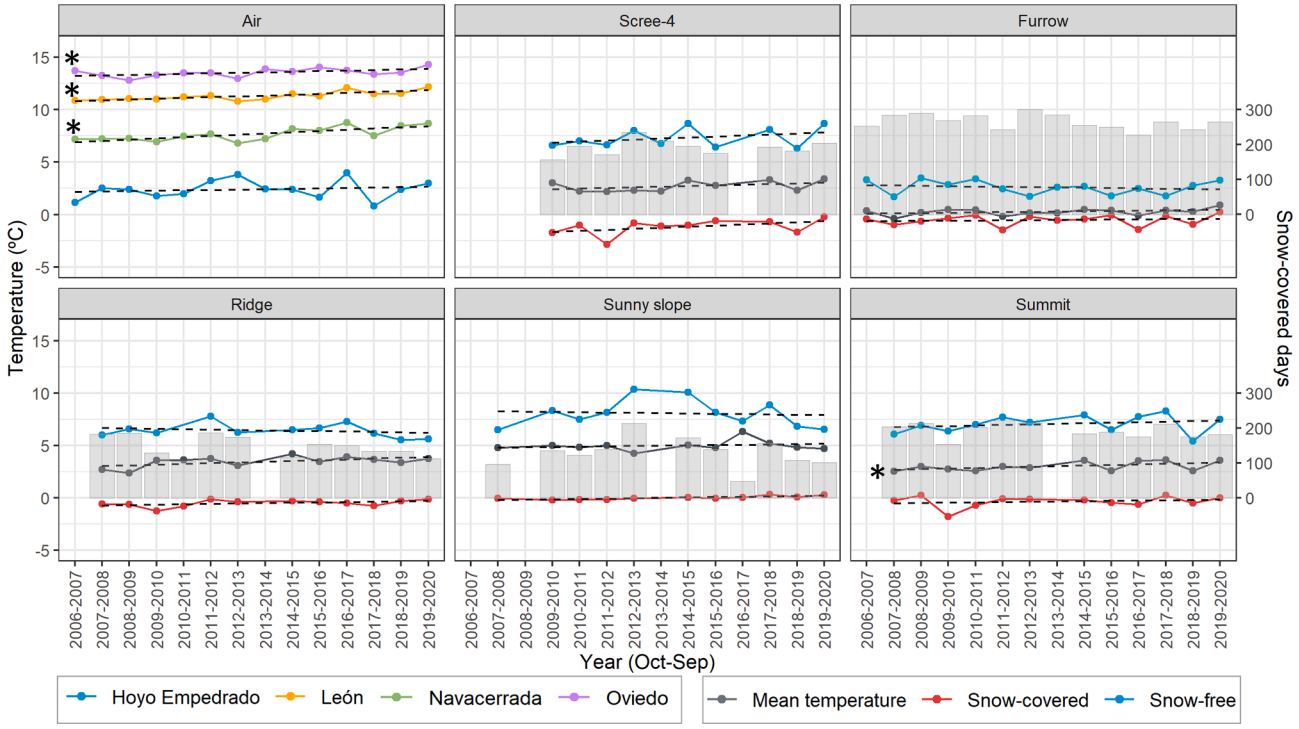

Fig. 3. Interannual GST evolution in each location, including snow-covered and snow-free periods, and AT in Hoyo Empedrado Cirque and some other reference official meteorological stations. Bars represent SCD. * indicates that the trend is statistically significant (p-value < 0.05, tested at 95% confidence level).

Sunny slope. The increase was higher (~0.06 °C per year) in Scree 4 and Summit. However, only the Summit values indicated statistically significant increasing trends from Mann-Kendall test (p value = 0.043, tested at 95% confidence level). The trends were similar in the snow-free and snow-covered periods: however, slight decreases in snow-free periods appeared in furrow, ridge, and sunny slope locations. Note that colder temperatures occurred during the snow-covered period, as snow is present in the coldest period of the year. MAAT showed higher variations than MAGST, while GST showed fewer differences during the snow-covered period than during the snow-free period. The limited data period reduces the significance of the data; however, reference AEMET meteorological stations (León, Navacerrada, and Oviedo) showed a higher increase (0.05 °C to 0.1 °C per year) with statistical significance during the same period (Fig. 3).

MAGST differences up to 2 °C were observed, being more relevant in the sunny slope and ridge. The lowest interannual difference in temperature was produced in the furrow of the rock glacier, where the difference between the coldest and the hottest year was 1.4 °C. Scree 1 and Root also had a low interannual thermal amplitude (0.7 °C and 0.9 °C, respectively), but the monitoring period was rather short. Conversely, the sunny slope presented a higher variation (from 4.3 °C in 2012–2013 to 6.3 °C in 2016–2017). Monthly thermal oscillation was also very reduced in the rock glacier furrow (4.7 °C) and increased progressively in this slope to 14.5 °C in Scree 1 and 13.6 °C in Root, which showed values similar to those in the northern slope of the cirque (Table 2).

4.2. Topoclimatic conditions and thermal behaviour of each site

Six dataloggers were located in the talus slope and in the furrow of the rock glacier developed at the foot: Root (highest part), Scree 4, Scree 3, Scree 2, Scree 1 and Furrow (the lowest part). There is a gradation in particle size in the talus slope, from gravels in Root to boulders up to 1–2 m in Scree 3 and up to 4–5 m in Scree 1 and Furrow locations. Solar radiation increased from the upper part to the talus apex. SCD and estimated thickness also progressively increased from Root to Furrow, varying between 266 days per year in Furrow to 193 days in Scree 4 and 209 in Root. Snow cover was usually continuous from November in Scree 1 and Furrow, but more discontinuous until January in the upper part of the slope (Fig. 4). In Root and Scree 4, snow cover persisted from mid-May to late June (something more in Root than in Scree 4). In Scree 1, the snow usually persisted until July, but only three years of data exist. In Furrow, snow melting occurred from July (28 June 2019) to late August (26 August 2013) and it was always the site with most persistence of snow. Snow depth estimation reports a mean of 7.1 m in this location, varying from 2.7 in 2019 to 10.8 m in 2013. Snow depth also decrease toward the upper part of the talus slope (5.6 m in Scree 1, 4.4 m in Scree 2, 3.5 m in Scree 3, 2.0 m in Scree 4), with a slight increase at the foot of the rock wall (3.2 m in Root) (Table 2).

A thermal inversion occurred in this slope, where the upper locations were the hottest, while the coldest located at the base. MAGST range from 2.4 °C (Root) and 2.8 °C (Scree 4) in the upper part, 1.7 °C in Scree 3, 1.0 °C in Scree 2, and 0.3 °C in Scree 1 and Furrow. The mean annual days with negative temperatures were also greater in Scree 1 and Furrow (Table 2). Mean monthly near-surface ground temperatures (MMGST) were negative from November to May in all of them, except in May in Root and Scree 4. During the summer, there were strong differences in MMGST; in August was 12.0 and 12.2 °C in the Root and Scree 4, 11.0 °C in Scree 3, 8.6 °C in Scree 2, 5.1 °C in Scree 1 and 2.6 °C in Furrow. In September, where snow was always absent and AT was lower, the differences were lower but also showed a clear thermal inversion. In winter months, MMGST was lower in the talus slope than in Furrow, but the coldest point varied. MMGST was below −2.0 °C in Scree 4 (December), Scree 3 and Scree 2 (December to February), and Scree 1 (February and March). The coldest months were February (Root and Scree 1), December (Scree 4, Scree 3 and Scree 2) and March (Furrow). In any case, important interannual differences existed during winter (Fig. 2), as temperatures could stabilise below thick snow cover at different temperatures. The mean annual freeze–thaw cycles varied from 10 (Scree 1) to 23 (Scree 3).

The rock glacier ridge showed a shorter snow-covered duration and lower thickness (mean 0.5 m, maximum 0.92 m) due to intense wind action. Even the winter period could be snow-free or have very little snow cover (Fig. 4), but some snow typically remains until mid-April to late May, with a mean of 152 SCD per year. MAGST was 3.3 °C, with negative MMGST for 5 months (November to March, April 0.01 °C). The mean annual number of days with negative temperature was 164, with 43 freeze–thaw days, the highest value of the study area. Summer reached average temperatures of 12 °C and 11.6 °C in July and August, respectively. Due to scarce snow cover, winter and spring cold penetration occurs, and this site showed higher thermal oscillation during winter months than most other locations (mean daily thermal oscillation 1.8 °C in March, 2.6 °C in April, 4.7 °C in May, while that in the scree was<0.5 °C in the same months). Frequent descents to −4 to −6 °C from November to April, which were rare in other locations, were observed.

The datalogger located on a sunny slope receives the highest annual potential solar radiation. Snow cover usually persisted during winter months, but some years (2007–2008, 2011–2012, 2015–2016, 2016–2017, and 2018–2019) was more discontinuous or isolated the ground from late January (Fig. 4). Instead, the cold penetration was quite low (mean minimum temperatures were the highest). Snow cover lasted from mid-April to late May (except 11 June 2013), summing a mean of 126 SCD, which was the minimum value of the study sites. In addition, the mean annual maximum thickness was 0.9 m; MAGST was the highest (5.0 °C) and the lowest number of days with negative temperatures (62) occurred, with 20 freeze–thaw cycles (Table 2). In this location, no month had negative average temperatures, although between January and March, the average temperature was below 0.5 °C. The average temperature exceeded 10 °C between July and September, reaching an average of 13.7 °C in August (Table 2).

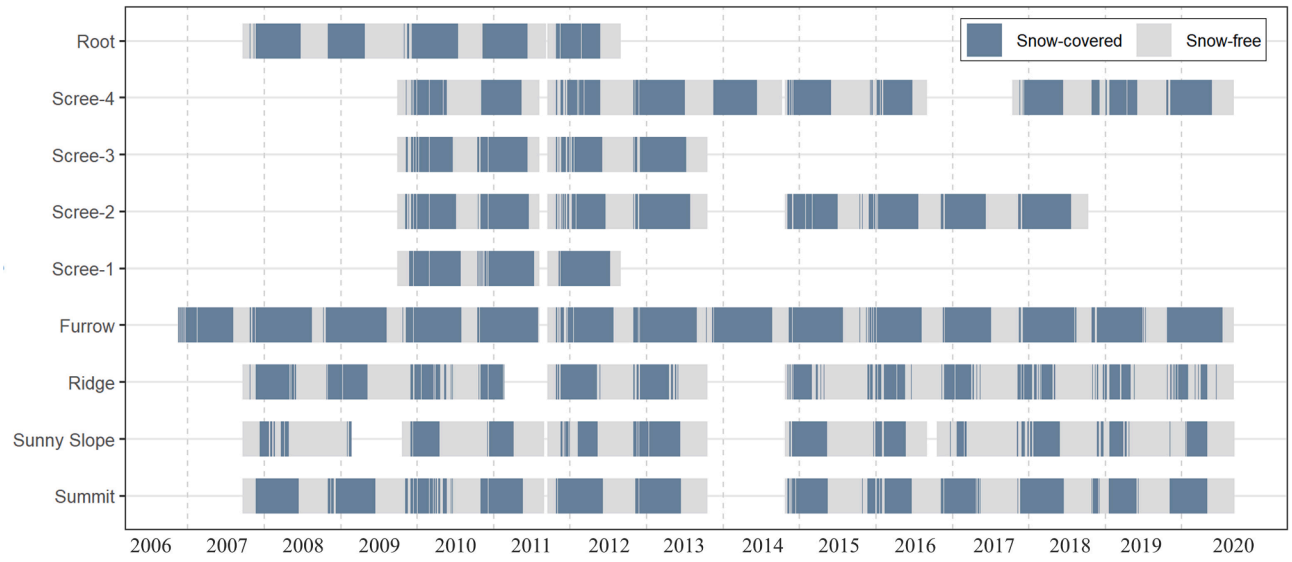

Fig. 4. Daily estimation of snow cover in locations obtained through temperature data-series.

Near the summit, at 2471 m altitude, there was a datalogger which received a large amount of solar radiation due to its orientation and the planar shape of this slope. The snow-covered period lasted from December to April (mean 194 days), with 2.1 m a mean snow depth. Usually, snow was continuous throughout the winter, but some years (i.e. 2009–2010) were more discontinuous (Fig. 4). Temperatures in late autumn could be very low (−5.0 °C) due to the lack of snow cover. Years with early snow cover (2008–2009, 2011–2012, 2017–2018, and 2019–2020) temperatures remained at 0 °C during all snow-covered periods. In contrast, during years with minimal snow in late autumn (2009–2010, 2018–2019) temperatures dropped following AT but with higher values (reaching −5.0 °C to −7.0 °C). Snow melting was complete from May (exceptionally 22 April 2017) to June (21 June 2016). When snow melts, temperatures rose considerably to exceed 10 °C on average in the months of July and August. Then, there was a progressive decrease in the average temperature until it remained again around 0 °C in November. The MAGST of Summit was 3.1 °C. The maximum temperature reached in August (MMGST 10.9 °C), and the minimum in January (MMGST −0.8 °C). Negative averages were recorded between November and March, although in April and May, the MMGST was below 1 °C. The mean annual number of days with negative temperatures was 145 (the second lowest value), with 19 freeze–thaw days (Table 2).

4.3. BTS measurements

The BTS data were obtained at 25 points on the scree and rock glacier, showing a temperature decrease towards the rock glacier furrow. Temperature was between −2 and −3.1 °C in the lower part of the scree and the rock glacier furrow, contrasting with temperatures between −0.6 and −2. °C in the upper part, usually around −1.5 °C (Fig. 5). In the sunny slope data was between 0.2 °C in the upper part and −0.5 °C in the lower part. The snow cover was between 0.63 and 2.65 m in the analysed area. In the cirque bottom measurements could not be performed because of snow cover depth greater than 3 m. This day, dataloggers located in the furrow and in the root registered −1.5 °C and −0.6 °C in the ridge.

4.4. Electrical resistivity tomography

The results of electrical resistivity tomography (Fig. 6) reveal the following:

a) A 3 to 10 m layer with high resistivity values (150.000 to over 60.000 Ohm.m), interpreted as the talus boulders, including numerous voids between them. In the furrow, high resistivity values were also located below 5 m depth.
b) Below debris, resistivity values were clearly lower, which could be related to the rock substrate and fine materials in the ridge.
c) Some lenses of higher resistivity were found in two areas: one located in the furrow below 5 m depth and another one close to Scree-2 location. Also, high resistivity lenses were found in the upper part of the talus slope, between Root and Scree-4.

5. Discussion

Beyond the limited altitudinal range analysed (2264–2471 m.a.s.l.), significant MAGST differences were registered, ranging from 0.3 °C to 5.1 °C, while MAAT was 2.3 °C in the same period (2006–2020). Similar MAGST differences have been observed in previous studies on mountain environments (Gubler et al., 2011; Rödder and Kneisel, 2012; Schneider et al., 2012; Thorn et al., 1999), indicating that local factors notably influence GST. In the study area, in addition to AT, the main factors controlling GST were substrate, solar radiation, air convection, and snow cover (Fig. 7). Higher temperatures occur in sunny slopes, summit, and ridges. These sites coincide with the higher solar radiation (sunny slope and summit) and fewer SCD (sunny slope and ridge) but also with the three points including fine-grained soils. In contrast, colder temperatures appear in the talus slope and the furrow, being a thermal inversion in this north-face slope, and the lowest temperatures are found in the furrow and are progressively higher to the upper slope. The role of each factor is discussed below.

5.1. The role of snow cover

As we have previously shown, SCD in Hoyo Empedrado Cirque

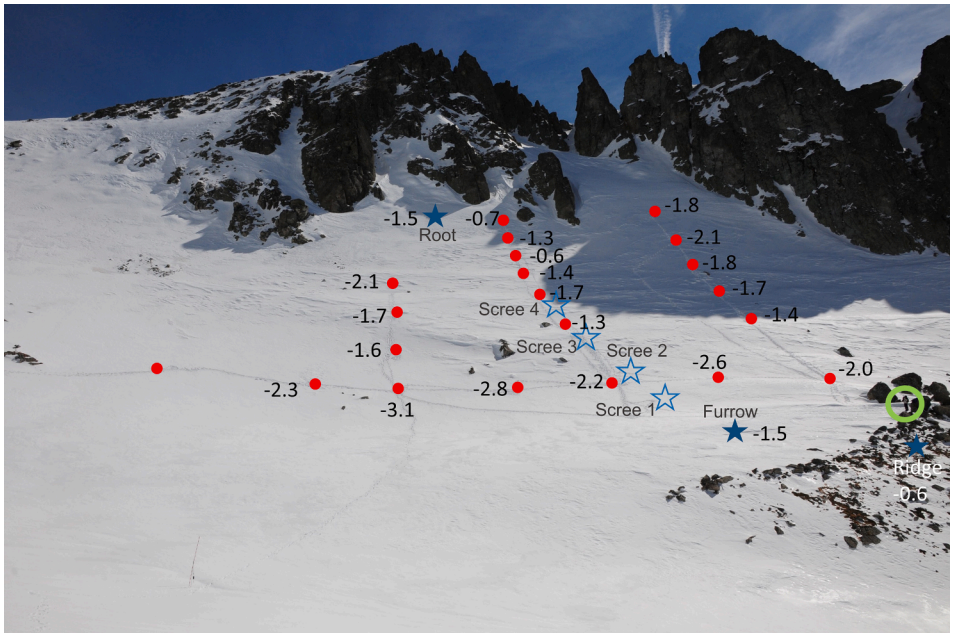

Fig. 5. BTS values 03 April 2009. Red circles represent BTS measurements while blue stars represent temperature registered in dataloggers (Root, Furrow, and Ridge) at the same hour. Green circle shows J.M. Redondo-Vega as scale. (For interpretation of the references to colour in this figure legend, the reader is referred to the web version of this article.)

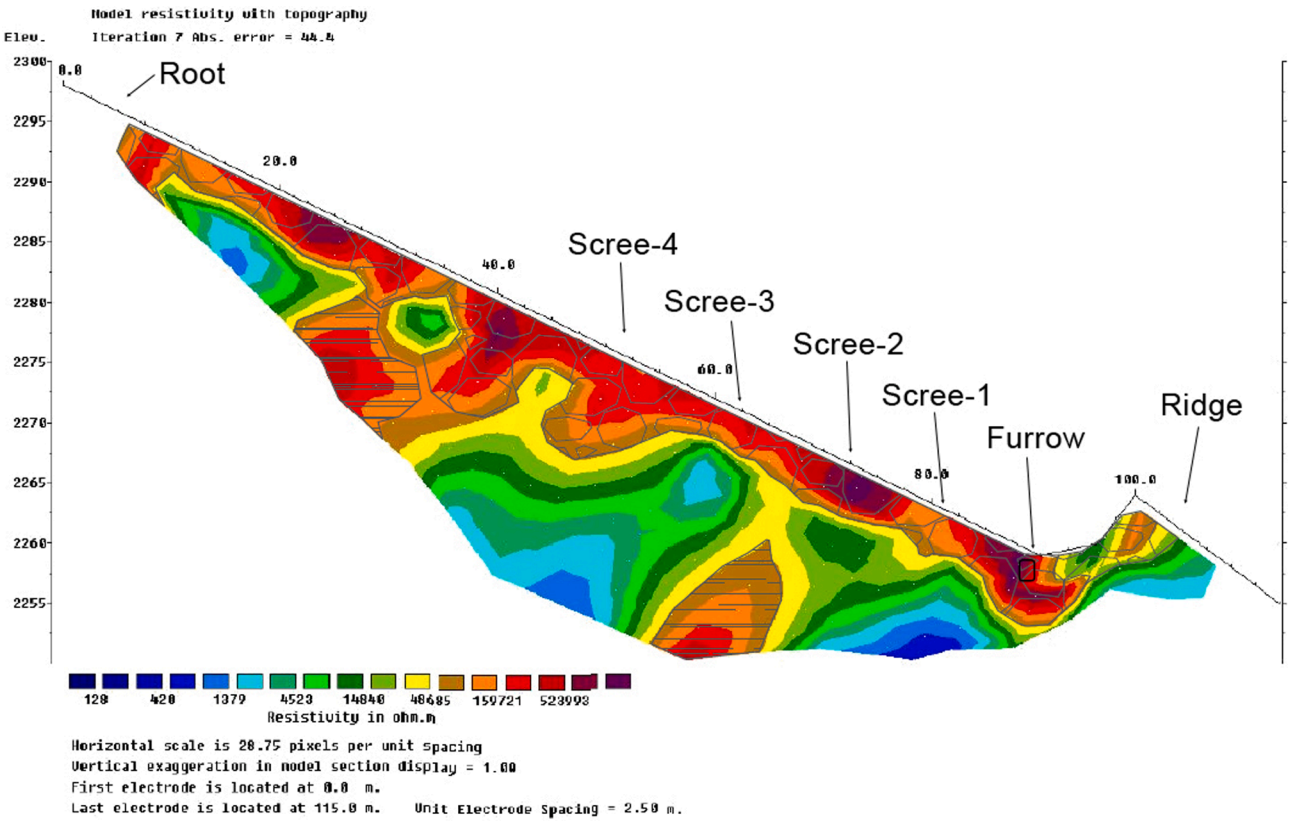

Fig. 6. Electrical resistivity tomography from the talus slope and protalus lobe on 13 September 2019.

ranged from 126 (minimum 48) to 266 (maximum 301) days depending on the location, being more persistent in the northern slope and especially in the furrow and scarcer in windy exposed areas, such as the ridge (Fig. 4). Snow depth over 0.8 m occurs in the talus slope, furrow, and summit, while this only occurs for some years in the ridge and the sunny slope. Maximum snow depth occurs in the furrow, reaching more than 6 m in most years (mean 7.1 m) (Table 2).

In the Hoyo Empedrado Cirque, the observed thermal differences correlate very well with SCD; therefore, snow cover seems to be the most relevant factor influencing GST, as observed in previous research (Hrbáček et al., 2020; Zhao et al., 2018). The longest period of snow cover the coldest temperature appears, with the furrow being the coldest place and the sunny slope being the hottest. The correlation between both variables is 0.85 (Fig. 8a), indicating that snow has a negative thermal offset with respect to AT. Similar results were obtained at different locations in the Peña Prieta and Picos de Europa massifs (Pisabarro et al., 2017) and all previous research in the Cantabrian Mountains has reported the strong dependence of GST on snow (Pisabarro, 2020; Pisabarro et al., 2015, 2017; Ruiz-Fernández et al., 2017; Santos-González et al., 2009). Although snow and temperature are partially controlled by solar radiation, the correlation between both factors is low (Fig. 8b), indicating that snow cover is more relevant than insolation in this case. The redistribution of snow by the wind seems to be more relevant than insolation (Fig. 8c), as snow accumulation is greater in topographically depressed areas. Snow cover depends on snow precipitation as well as on melting and redistribution by wind, being affected by the relief, geomorphological processes, vegetation or micro-relief, and micro-climate, which are strongly variable in space and time (i.e. Elder, Dozier and Michaelsen, 1991; Mott et al., 2010; He and Ohara, 2017).

However, the role of snow is complex and differs throughout the year (Ling and Zhang, 2003; Yu et al., 2004). In autumn, an early snow cover (last October–early November) caused GST to reach 0 °C while the AT usually dropped significantly below 0 °C. In this case, the insulating effect of snow prevents cold penetration in the ground, as previously noted (Ishikawa, 2003). In contrast, the delayed appearance of a thick snow cover usually cause lower GST because AT is generally low. Previous research (Luetschg, Lehning and Haeberli, 2008; Santos-González et al., 2009; Rödder and Kneisel, 2012; Marmy et al., 2013; Haberkorn et al., 2015) noted that a delay in the appearance of a non-insulating snow cover could make colder the ground thermal regime of the entire snow-covered period, as it promotes cold penetration in the ground and snow isolates the ground that maintains cold air independently if the remainder of the winter is cold or mild. Likewise, a thin and discontinuous snow cover can noticeably accelerate the exothermic process of the ground, producing a cooling effect on the shallow soil (Zhao et al., 2018). In the Hoyo Empedrado Cirque, the delayed appearance of snow is well correlated with colder temperatures in February and March in some locations (Supplementary data 1), especially in the talus slope. But is not correlated in the ridge (where snow thickness is usually low and exerts less insulating effect) and in the furrow, where thick snow cover use appears earlier. In any case, these data agree with the general statement that the delayed appearance of snow cover favours cold penetration in the ground.

In winter, thick snow usually covers the whole cirque, but in some years, minimal snow was observed, particularly in January. Temperatures tended to be constant around 0 °C, while AT was typically lower, but positive AT during the winter period have been observed every year. In windy-exposed locations, such as the ridge, intense cold penetration occurs during winter. Rain during winter sometimes occurs at this altitude but does not exert a strong influence on GST. In contrast, some episodes have relevant consequences for GST. For example, during 18–19 January 2013, the explosive cyclogenesis 'Gong' promoted a sudden increase in GST that persisted during the rest of the snow-covered period instead of air temperature decreases (Fig. 9a). In addition, the explosive cyclogenesis 'Gabriel' on 30 January 2015 produced

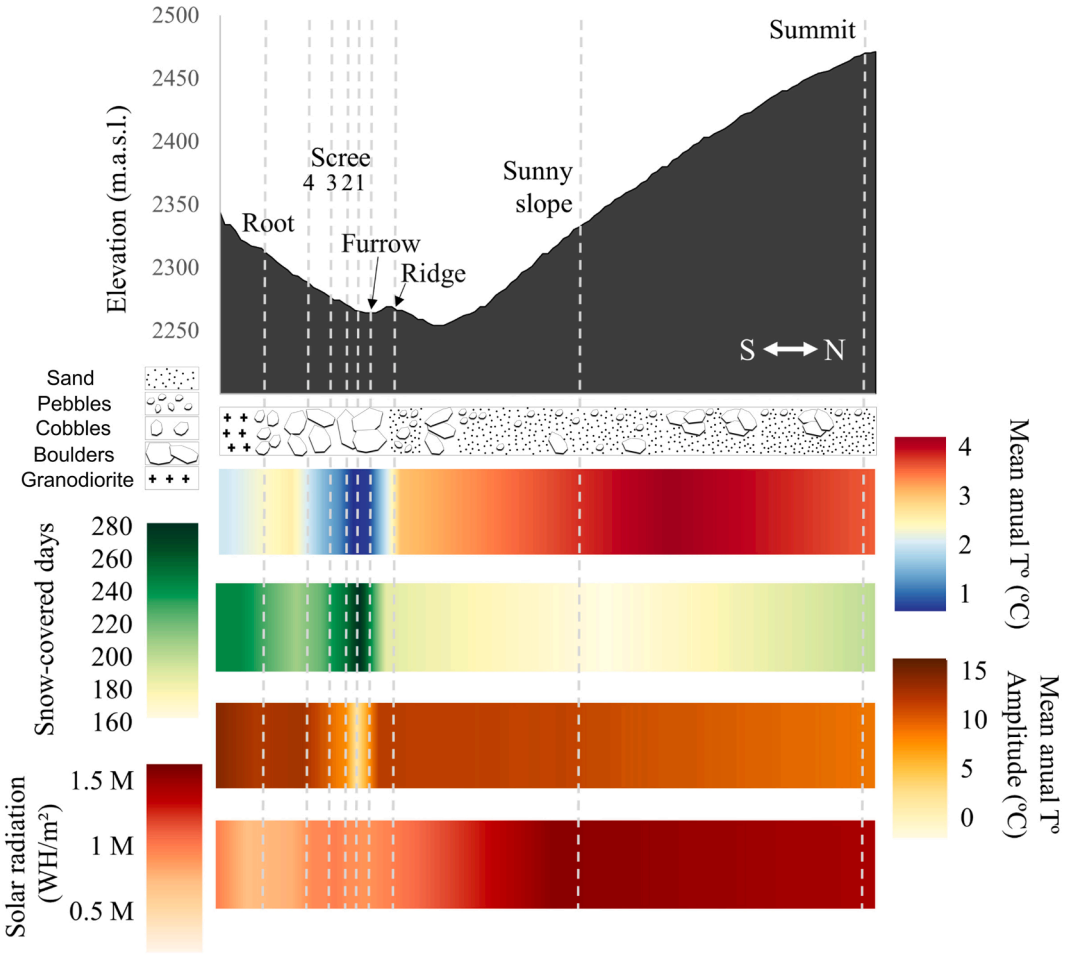

Fig. 7. MAGST, SCD, mean annual temperature amplitude, and solar radiation in a topographic study area profile.

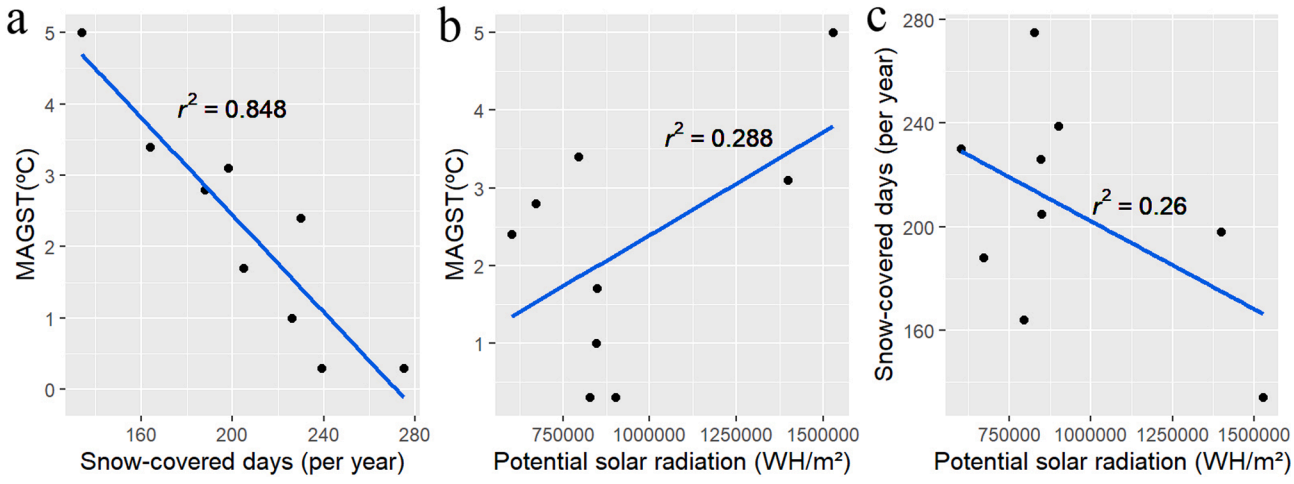

Fig. 8. Correlations between MAGST, SCD inferred by GST, and potential solar radiation in studied sites.

relevant changes in GST (Fig. 9b). The impact of these winter rain-on-snow events on the GST regime has also been noted in other cold environments (Strand, 2016; Westermann et al., 2011).

During spring, long-lasting snow contributes to the zero-curtain effect (Outcalt et al., 1990), persisting until the snow melts, as previous works reported (Ishikawa, 2003). It is usually referred to as wet, medium-textured mineral and organic soils during freezing (Harris and Corte, 1992), but occurs in all locations, including the talus slope. The appearance of the zero-curtain effect has been reported quite frequently in openwork deposits (Hanson and Hoelzle, 2004; Santos-González et al., 2009; Sawada et al., 2003; Zacharda et al., 2007).

In the Hoyo Empedrado Cirque in some years, GST stabilises around 0 °C with the first snow and persists during winter and spring (Furrow 2010–2011, from 31 October to 30 July; Sunny slope 2014–2015, from 30 November to 12 May). However, the zero-curtain effect typically emerges when snow starts melting. The initiation of this process is

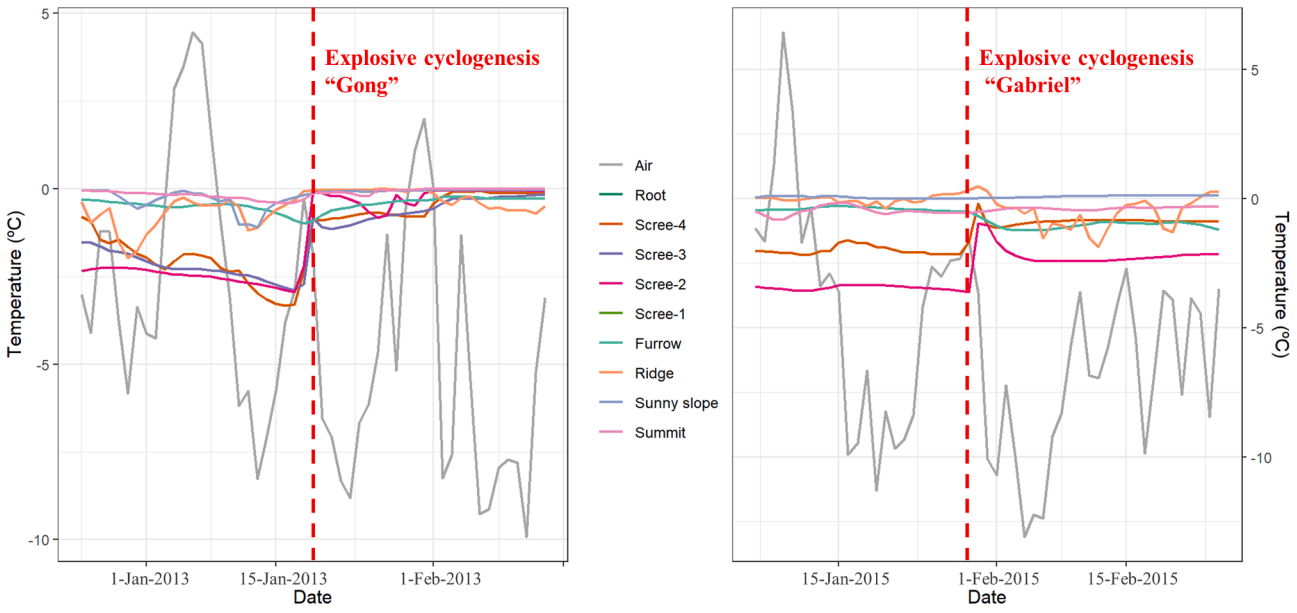

Fig. 9. Effects of explosive cyclogenesis 'Gong' (a) and 'Gabriel' (b) in the GST of the Hoyo Empedrado Cirque. Note the abrupt change in temperature pattern in most locations.

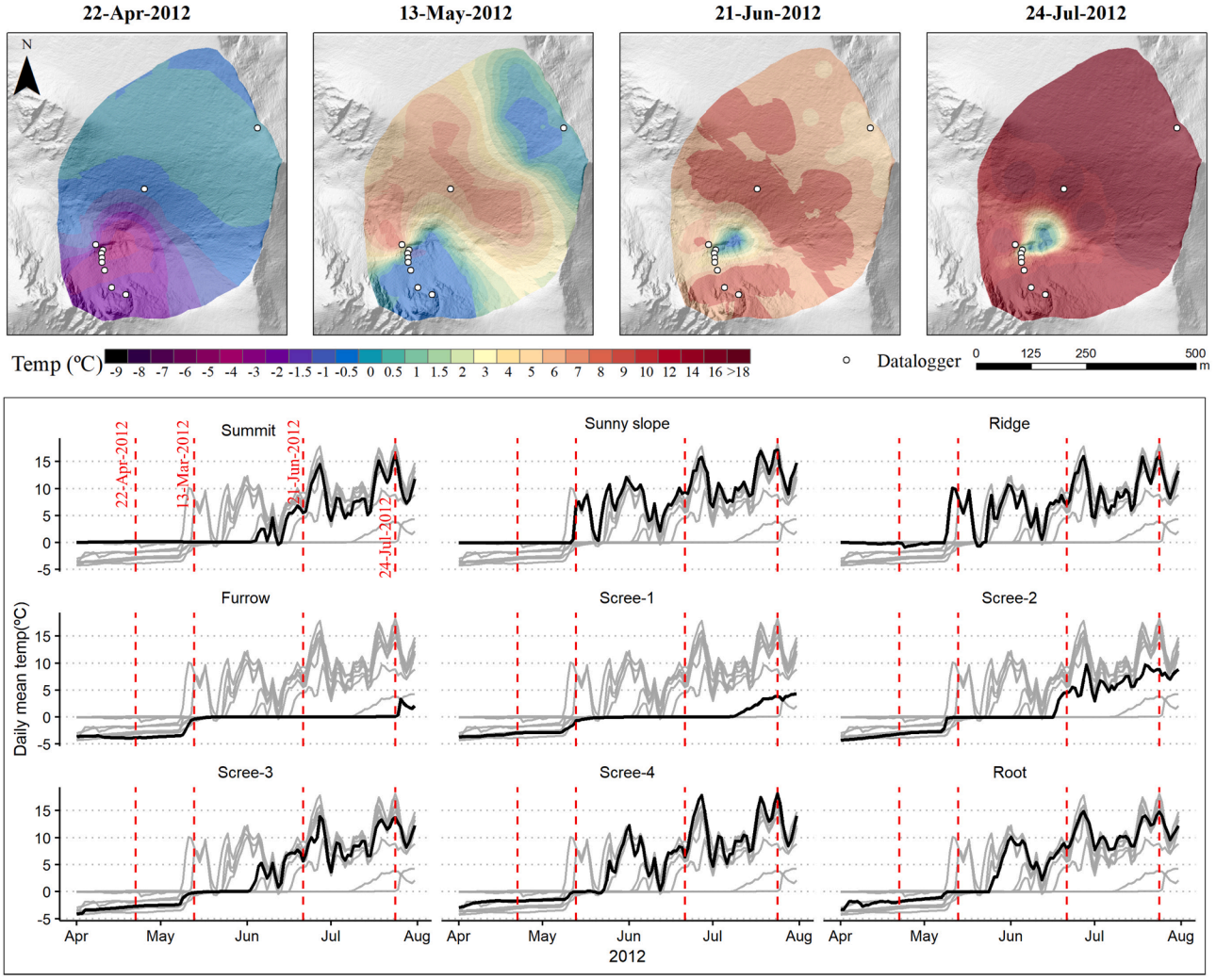

Fig. 10. Temperatures during 2012 spring and early summer in the Hoyo Empedrado Cirque. Note different periods of zero curtain effect in each location. This effect ends when snow melts and occurs in different dates depending on location; hence, snow favours cold GST.

primarily controlled by AT and solar radiation (Ohmura, 2001) as well as by the percolation of rain, snow surface runoff, and refreezing of meltwater (Ishikawa, 2003; Senese et al., 2014; Westermann et al., 2011). The zero curtain effect starts in the summit and sunny slopes from mid-February to mid-April and in the talus slope and furrow from April to mid-May, ending from the end of April (sunny slope) to late July or August (furrow) (Fig. 10). These differences are likely related to various levels of insolation during the spring. The south face receives more solar radiation and snow melts earlier than in the north face. The end of the melting period is controlled by snow thickness. In the furrow, up to 5–7 m of snow often accumulates, leading to a very long zero curtain duration (up to 100 days; Fig. 10) and a high value compared to other mountainous areas (Staub and Delaloye, 2017).

During the spring, AT usually is over 0 °C (MAAT: May 4.2 °C, June 7.7 °C); therefore, snow preserves cold GST until snow melts. In that sense, the snow melting day plays an important role in MAGST, as differences could be very important depending on locations and years, varying from April to September (Fig. 4). Early melting caused the ground stop to be isolated from the AT earlier; therefore, this cause an increase in GST as positive temperatures are registered earlier, as noted in a previous study (Sysolyatin et al., 2020). In contrast, a long-lasting snow cover retarded ground warming, as isolated from relatively high temperatures during this period (Zhao et al., 2018), contributing to the preservation of permafrost (Magnin et al., 2017). Some authors have noted that the cooling caused by delayed snowfall in autumn is within the same order of magnitude as the effect of delayed snowmelt in spring (Ling and Zhang, 2003; Luetschg et al., 2008). In any case, in the Hoyo Empedrado Cirque, there is no correlation between the snowmelt day and MAGST, indicating that other factors may be more relevant.

5.2. *Influence of substrate and air circulation in the talus slope*

The substrate seems to be the other more relevant factor influencing GST in the study area. In the Hoyo Empedrado Cirque, the coarse deposits are located in the north face of the cirque, where snow cover is higher and temperatures are lower (Fig. 7). However, some data have indicated a cooling effect of the substrate. Fine-grained soils (ridge, sunny slope, and summit) usually show higher GST than AT, especially during SCD. At these sites, when thick snow exists, snow prevents cold penetration during winter. In contrast, in the talus slope and the rock glacier, GST in the snow cover period is usually below AT, indicating a cooling effect with respect to the fine-grained soils, instead of the snow isolate from AT.

During the snow-free period, Ridge and Summit show variable patterns, with GST 1.5 °C lower or higher than AT, while in the sunny slope, GST is up to 4 °C higher than AT (Fig. 11). In the talus slope, GST is generally lower than AT, except for some years in Scree 4 and Root (i.e. the upper part of the talus slope). The greatest differences between GST and AT appear in the furrow, where GST is 3–6 °C lower than AT in the snow-free period, showing cold summer conditions (Fig. 11).

These data agree with previous observations in other mountain environments with colder temperatures in blocky surfaces than in fine-grained soils (Harris and Pedersen, 1998; Juliussen and Humlum, 2008; Onaca et al., 2015; Rödder and Kneisel, 2012; Yu et al., 2004).

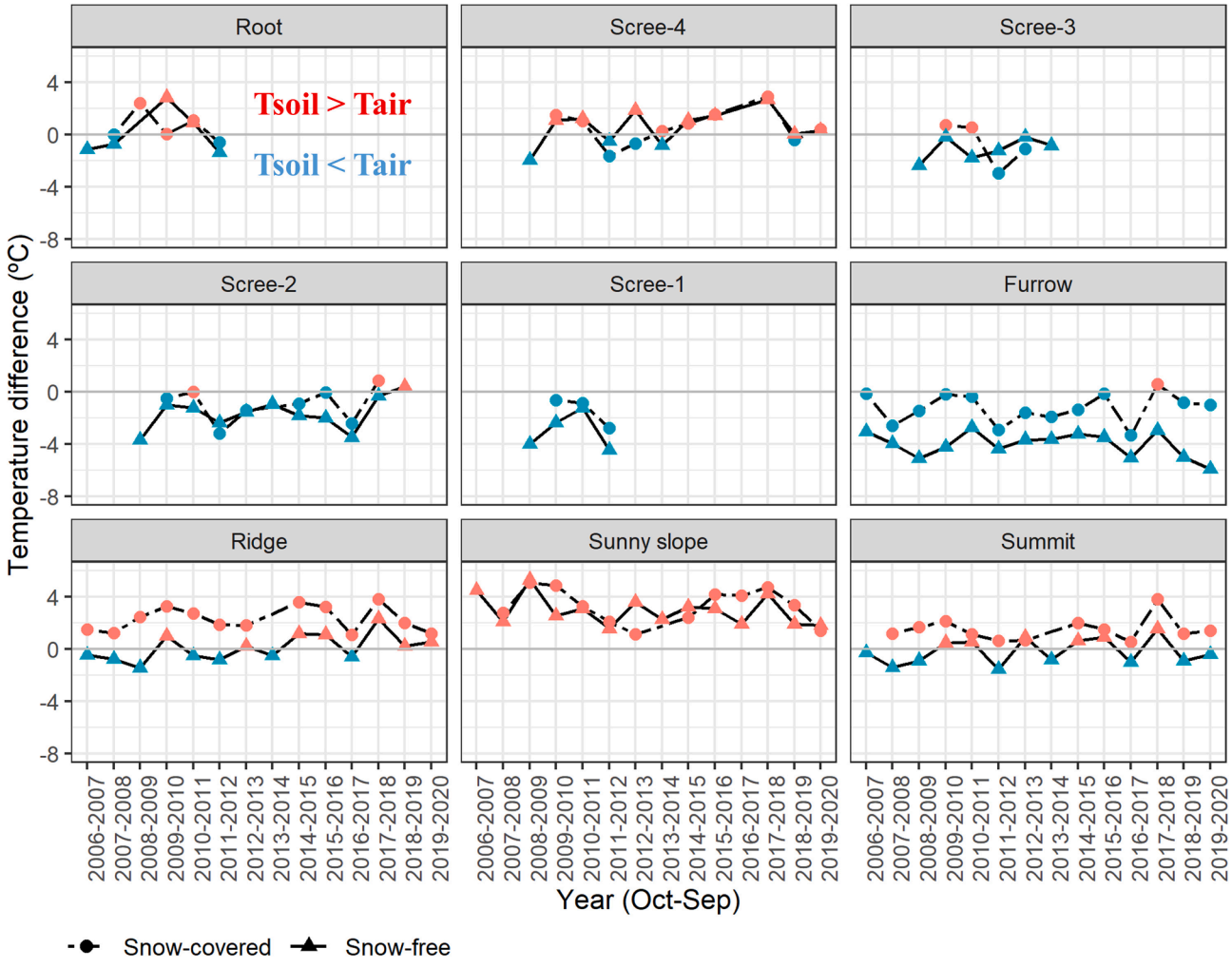

Fig. 11. Differences between AT and GST during snow-covered and snow-free periods per year in each location.

This cooler effect is more significant during the snow-free period, while the heater effect of the fine-grained soil was higher during the snow-covered period. Coarse block layers exert a cooling influence in GT due to 'a) temperature-driven convection of air, b) a reduced warming effect of the winter snow, and c) the advection of latent heat by snow that enters deep into the voids' (Gruber and Haeberli, 2009).

Relevant differences between GST in the talus slope and rock glacier indicate that, among snow cover influence, solar radiation, and substrate, other influences explain temperature differences. Several studies have observed air circulation below the snow cover in talus slopes and rock glaciers, mainly in permafrost areas (Delaloye et al., 2003; Delaloye and Lambiel, 2005; Hanson and Hoelzle, 2004; Harris and Pedersen, 1998; Morard et al., 2010; Popescu et al., 2017; Sawada et al., 2003; Schneider et al., 2012; Wicky and Hauck, 2020). This cooling mechanism is more effective with minimal snow, as thick snow cover can reduce or inhibit convection (Gruber and Haeberli, 2009).

In the Hoyo Empedrado rock glacier and the talus slope, temperatures in early winter use to be lower in the upper part of the scree. The opposite occurs at the end of winter, when the coldest air is present in the furrow. In some seasons, a progressive temperature increase in the upper part and a progressive decrease in the lower part can be inferred from the graphs. Fig. 12 illustrates a cold period during January 2012 that affects most of the scree sites, which show lower temperatures than the furrow. During February and March, the temperature of scree dataloggers increased, while the furrow descended. In April, the lowest temperature was recorded in the furrow, and the temperature was progressively higher in the upper part of the talus slope. This pattern reveals air convection inside the talus, as the so-called chimney effect, described by Wakonigg (1996) and observed in several studies. In approximately half of the studied years, air convection (i.e. progressive temperature decreases in the lower part of the slope) was observed in the GST data.

We did not observe warm funnels at the top of the slope (Sawada et al., 2003) and GST in this part of the talus is negative at the end of the winter; therefore, there is no clear evidence of hot transfer to the upper part of the slope. This could be related to the warmer winter compared to other climate areas. For example, Morard et al. (2010) observed that during the mild winter of 2006–2007, the ground was not affected by intense cooling. Probably the ascending air circulation is less efficient due to a weak temperature gradient between the outside air and ground temperatures. The reduced size of the slope and the small thickness of the debris deposit could also contribute to limiting air movement with respect to thicker talus slopes.

During the snow-free period (July-August to October-November), cold air persisted in the lower part of the talus slope (Scree 1 and Furrow). MGST in September was 3.5 °C in Furrow, 5.0° in Scree 1, 5.9 °C in Scree 2, 7.0 °C in Scree 3, and 7.4 °C in Scree 4, showing a clear thermal inversion. Fig. 13 shows an example from the summer of 2010. This pattern is consistent with the thermal behaviour model proposed for talus slopes (Morard et al., 2010; Wakonigg, 1996; Wicky and Hauck, 2020), where the gravity discharge of cold air to the talus slope base occurs, despite higher potential solar radiation in the lower part of the scree. Therefore, the low thermal conductivity of the block layers produces a cooling effect with respect to fine-grained soils (Gruber and Haeberli, 2009).

These winter and summer processes contribute to the cooling effect in the lower part of the talus slope and the rock glacier furrow (Morard et al., 2010; Onaca et al., 2020; Popescu et al., 2017; Raska et al., 2011;

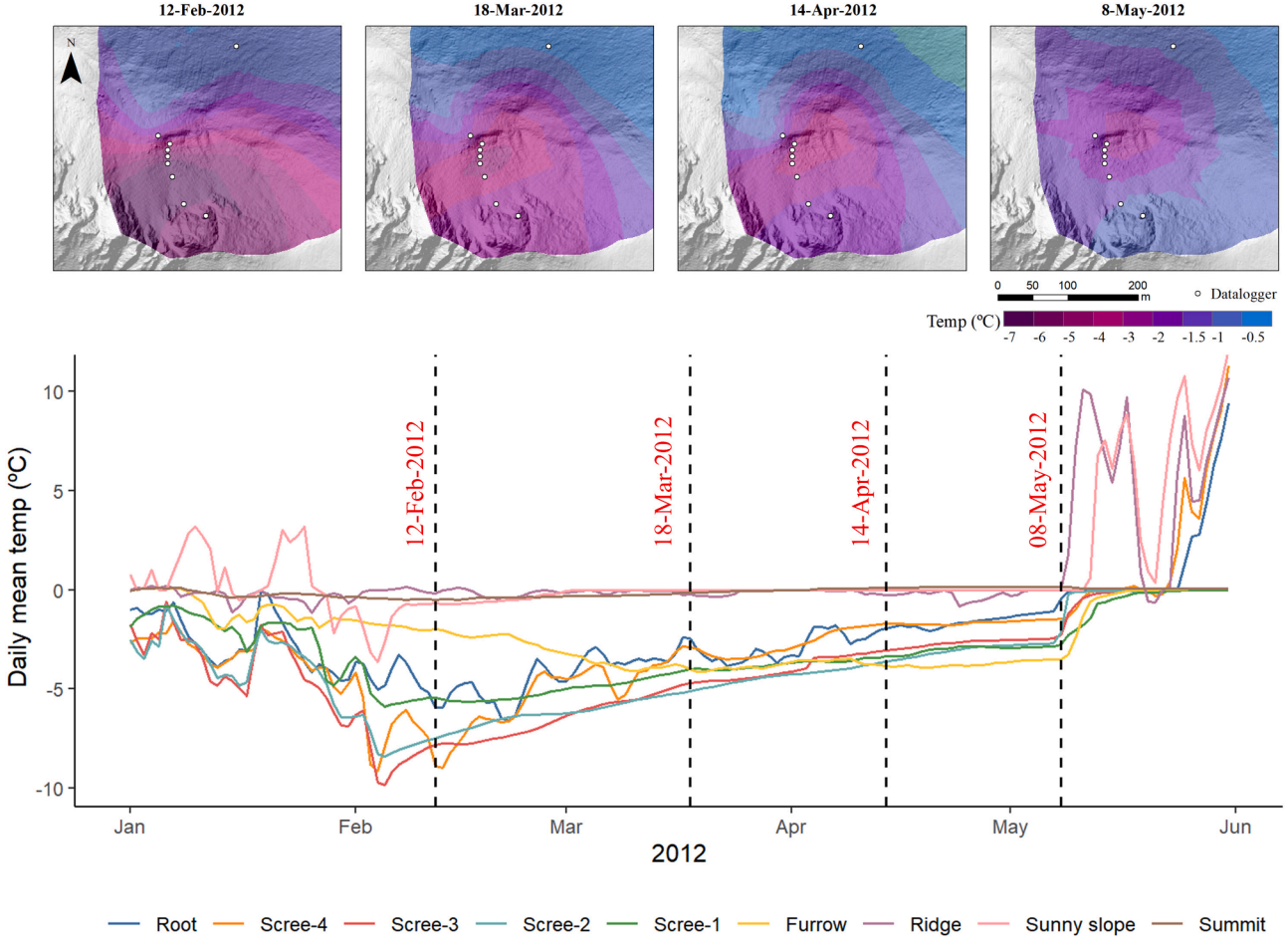

Fig. 12. Example of air circulation inside the talus slope and progressive cooling of the Furrow location in 2012.

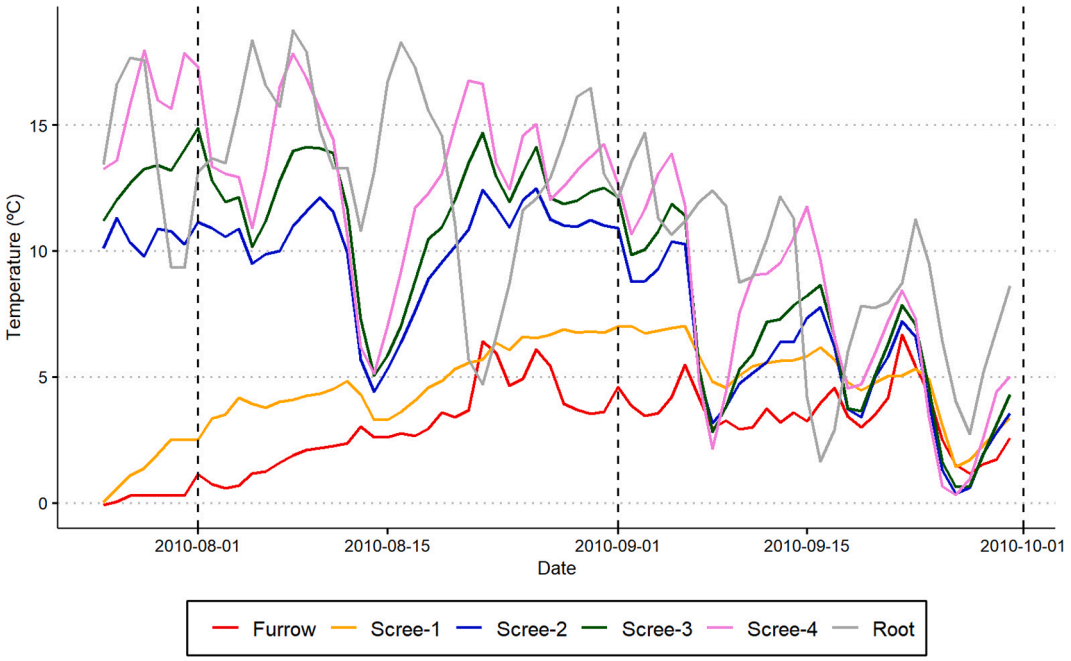

Fig. 13. Summer temperatures in the talus slope and the furrow of the rock glacier.

Wicky and Hauck, 2020).

5.3. Interannual variations, trends, and implications for BTS measurements

Relevant inter-annual differences in GST have been noted in previous research in mountainous areas (Kellerer-Pirklbauer, 2019; Kenner et al., 2017; Morard et al., 2010; Onaca et al., 2020; Staub et al., 2015; Sysolyatin et al., 2020), mostly related to snow cover. Although there is a good correlation between SCD and GST, in the 14 years record, there was no correlation in each site between annual SCD and MAGST each year, neither with a delayed first snow isolation appearance or disappearance and MAGST, indicating the complexity of the GST regime. There was also no correlation between air and ground temperature each year (Supplementary data 1). Thus, snowy years do not necessarily involve low GST, and cold years do not necessarily involve low GST as multiple factors interact.

The high variability at the end of the winter GST is a relevant factor. In alpine regions, particularly in the Alps (Brenning et al., 2005; Hoelzle, 1992), BTS temperatures have been used for the rapid detection of permafrost conditions, assuming that snow isolates GST from the air and temperature reflect subsurface conditions. This technique has also been used in the Pyrenees (Julián and Chueca, 2007; Serrano et al., 2020, 2019) and the Cantabrian Mountains (Serrano and González-Trueba, 2004) to detect possible permafrost conditions. In the Hoyo Empedrado Cirque, snow thickness is sufficient to apply the BTS method in most of the cirque and thermal values tend to be the lowest in the rock glacier furrow at the end of winter temperatures. However, analysing inter-annual differences between February and April reveals notable differences each year, with temperatures ranging from 0.2 °C to −4.0 °C. Thus, the likelihood of permafrost in the furrow as determined from BTS data are probable (<−3.0 °C) for 2 years, possible (−2.0 to −3.0 °C) for 2 years, and improbable for 10 years, with important temperatures differences (Fig. 14). The same inter-annual variability occurred in the upper part of the talus slope (Scree 4).

These relevant temperature differences at the end of the winter, when snow cover is very thick, indicate that other factors, such as early winter temperatures and air convection, play an important role in GST. One-year BTS measurements depend on the thermal regime of that year, that could or could not be representative of this site. A clear conclusion

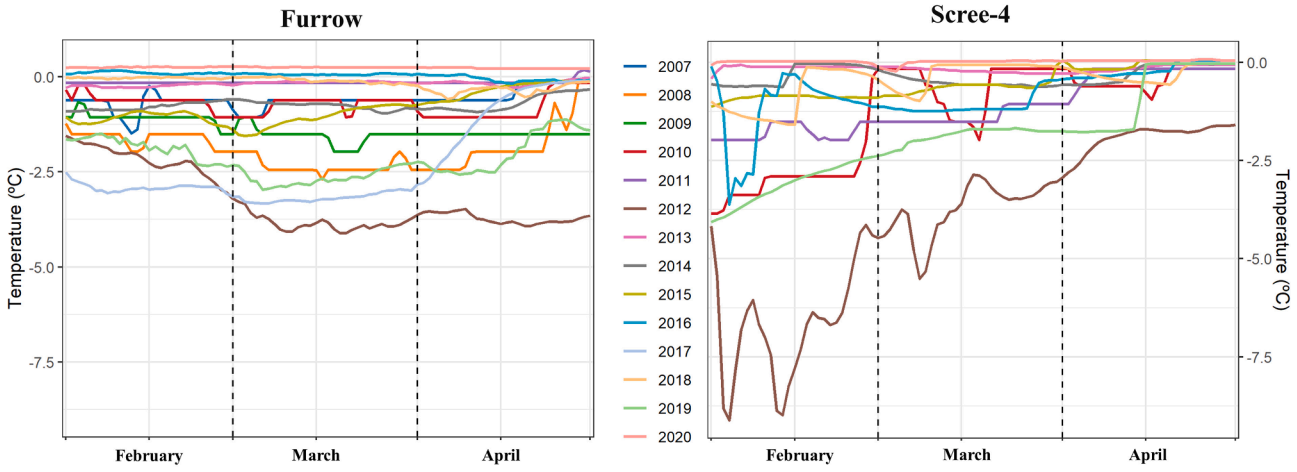

Fig. 14. Interannual GST variations form February to April in the Furrow and Scree 4 locations.

from these differences is that interpretation of the BTS data should be made very carefully because among other limitations (Ishikawa and Hirakawa, 2000), great inter-annual temperature differences could occur, as previously noted in the Alps (Kellerer-Pirklbauer, 2019).

5.4. Permafrost occurrence?

Permafrost appears in the high mountain environments of some Mediterranean mountains (Oliva et al., 2018). In the Iberian Peninsula, permafrost has been observed in Pyrenees above ~ 2600 m (Fernandes et al., 2018; Lugon et al., 2004) and one cirque of Sierra Nevada (Gómez-Ortiz et al., 2019) deglaciated during the 20th century. In the Cantabrian Mountains, relict permafrost related landforms are widespread, indicating permafrost conditions during the last glacial cycle and in some cases during the LIA (Gómez-Villar et al., 2011; Oliva et al., 2018). However, present-day permafrost occurrence has not been documented, except in the proximity of ice patches in Picos de Europa (Pisabarro et al., 2017) and the regional limit is probably close to the highest summits. In maritime climates, glaciation is at a similar altitude or lower than the lower limit of permafrost (Gruber and Haeberli, 2009). The Cantabrian Mountains have a transition climate from maritime to Mediterranean; therefore, both altitudes are probably similar, and permafrost, if present, is restricted to very few areas. In any case, the complex distribution of permafrost in mountainous areas and the difficulties in detection (Etzelmüller, 2013; Gruber and Haeberli, 2009; Haeberli et al., 2011) do not permit a clear view of possible permafrost distribution in the Cantabrian Mountains.

In the Hoyo Empedrado Cirque, temperature data exclude the existence of permafrost in most of the locations, but not in the furrow and the lowest part of the scree, where MAGST is 0.3 °C (Table 2). Some works has been found permafrost with MAGST over 0 °C or close to this temperature in the sporadic discontinuous zone (Haeberli et al., 2011; Lewkowicz et al., 2011; Throop et al., 2012), especially in present-day conditions, when permafrost is warming (Biskaborn et al., 2019).

BTS measurements in 2009 show that this is probably the coldest area of the cirque (Fig. 5). This area shows more favourable conditions in terms of topography, substrate, and snow cover for permafrost existence, according to the model of permafrost distribution in talus slopes (Haeberli, 1975; Lambiel and Pieracci, 2008), indicating that the coldest temperature and, where permafrost is present, the highest resistivity values are found in the lower part of the slopes. This is the case of the previous studies in similar areas that has been found low-altitude permafrost in talus slopes in alpine areas (Delaloye et al., 2003; Kellerer-Pirklbauer, 2019; Kneisel et al., 2000; Scapozza et al., 2011; Stiegler et al., 2014), where MAAT is usually higher than in the Hoyo Empedrado Cirque.

The role of air circulation inside the talus slope seems to be the most probable causal factor influencing this temperature pattern, explaining the progressive cooling during the end of the winter and the maintenance of cold air in the summer, as observed in the referenced works. Sawada et al. (2003) report that 'in the spring, snowmelt water flows to the valley bottom and refreezes, adding superimposed ice onto the perennial ice that fills the voids between coarse blocks', indicating that it is possible that this process also occurs in the Hoyo Empedrado Cirque.

The rock glacier and the talus slope do not show any signs of movement and previously was considered relict (Gómez-Villar et al., 2011; Redondo Vega et al., 2011). However, similar considered relict landforms has internal ice favoured by density-driven air flow (Colucci et al., 2019).

The ERT conducted on the talus slope and rock glacier (Fig. 6) showed very high resistivity values in the furrow, where the colder temperatures were registered. These values are consistent with the alpine permafrost, which usually exhibits higher values than the surrounding materials. In any case, a wide range of values have been found depending on the permafrost conditions (Mollaret et al., 2019). However, the high values also registered in the rock glacier surface, and probably related to voids between the very large boulders, makes the results unclear, as the higher values in the furrow could also be attributed to voids.

So no definitive evidence of permafrost has been found considering the following:

- MAGST is compatible with discontinuous permafrost in the most favourable area for permafrost conditions (i.e. the lowest part of the scree and the furrow of a small rock glacier).
- GST at the end of winter (March-April) is compatible with permafrost some years but not others.
- Summer temperatures are very low in Furrow and Scree 1 locations, which may be related to 'chimney effect'.
- Permafrost-related landforms appear; however, the large size of the boulders and the stability of the landforms prevent creeping movements independently whether internal ice appears or not.
- ERT exhibits higher resistivity values (compatible with permafrost) in the furrow, where the lowest temperatures were recorded. However, the values could also be related to voids, and the values were similar to those obtained in some other surficial parts of the talus slope.
- The small thickness of the deposit possibly difficulties permafrost maintenance.

Considering this, the presently evaluated data indicate the probable existence of permafrost; however, future work is required to analyse this site. If permafrost occurs, it will be the first reference to an inactive (or pseudo-relict) rock glacier in the entire Cantabrian Mountains.

6. Conclusions

The Hoyo Empedrado Cirque has been proven to be an interesting site for observing GST differences in mid-latitude mountainous areas due to notable contrasts in substrate, snow cover, and solar radiation. Hourly temperature data from 2006 to 2020 in nine locations revealed significant spatial and inter-annual GST differences. MAAT was 2.3 °C in that period; however, MAGST varied between 0.3 and 5.1 °C, indicating that the ground could have a positive or negative thermal offset. These differences are very well correlated with snow cover: in the sites with the longest snow cover duration, the lowest temperature appears. Days with negative maximum temperatures are over 220 in the coldest locations and drop significantly on the sunny slope (62). Freeze-thaw cycles are infrequent (10–43) and likely have very low geomorphological significance.

Snow is the main factor influencing the GST pattern, as it partially or totally decouples the ground from AT. Estimated snow cover duration varies from 126 to 266 mean days per hydrological year and estimated mean maximum thickness varies from 0.5 to 7.1 m. Topography and redistribution of snow by wind action seem to be the most important factor controlling snow cover, as solar radiation show less influence. Owing to the great snow cover differences, notable variations in the duration of the zero-curtain effect were observed. In the snowiest sites, the zero-curtain effect last for more than three months, until the snow completely melts. A delayed appearance of snow during late autumn and early winter favoured cold penetration in the ground and in some locations and years; this cause ground cooling throughout the snow-covered period, regardless of whether the remainder of the winter is cold or mild. During late winter, snow cover is thick but is highly variable depending on the year; therefore, one-year BTS values could have little significance in determining the ground thermal regime. The existence of extreme events (i.e. explosive cyclogenesis) promote changes in the GST regime throughout the entire snow-covered period, independent of the rest of the winter AT. The longest snow-covered period in spring and summer, the colder GST appears, as snow isolates the ground from the warm temperatures of this period. In any case, these factors explain interannual temperature variations, indicating complex

influences in the GST regime.

The colder influence of blocky surfaces has been proven in the Hoyo Empedrado Cirque, as the coarse blocky sites show lower temperatures than AT and the opposite tends to occur in fine-grained sites, especially during the snow-covered period. Air convention within the talus slope was observed based on the temperature data. During winter, cold air tends to progressively accumulate at the base of the slope but not all years seem to occur. During summer, the effect is more effective, with some degrees colder in the lowest part of the slope than the upper one. Because of this, in the talus slope, a clear inverse gradient occurs, with the furrow and the lower part of the scree being the coldest.

MAAT interannual differences over 3 °C were observed during the 14-y period. GST variations are less important but exceed 2 °C in some locations, indicating annually variable conditions. During this period, a slight positive temperature trend (0.03 °C to 0.06 °C per year) was observed at all sites, but only the Summit indicated statistically significance and the positive trend were less prominent than reference official meteorological stations, indicating that local topoclimatic conditions reduce the more global positive temperature trend.

GST in the lower part of the scree and furrow are compatible with the existence of permafrost. The ETR showed very high resistivity values in the rock glacier furrow. These values could be related to internal ice (permafrost) in the rock glacier; however, further analysis is necessary to confirm or discard permafrost occurrence.

The GST pattern distribution could be extrapolated to other Mediterranean and Oceanic glacial cirques in mid-latitude regions; however, changes in slope, boulder characteristics, talus slope thickness, snow cover duration and characteristics, and climate could introduce notable differences. For example, colder winter temperatures in more continental climates promote colder GST and less snow densification, factors that notably influence GST. Among these, future research on the influence of snow distribution, thickness, and density on GST, among the role of air thermal inversions, is necessary for a better understanding of temperature patterns.

Data availability

All temperature data related with the text could be visualized in the following url: https://buleria.unileon.es/handle/10612/12795.

Declaration of Competing Interest

The authors declare that they have no known competing financial interests or personal relationships that could have appeared to influence the work reported in this paper.

Acknowledgements

This research was supported by the project LE080G19 (Paleo-environmental significance and relationship with the global change of the Cantabrian Mountains rock glaciers: relative age dating and analysis of the internal structure using electrical tomography), founded by the Junta de Castilla y León, and previously by projects CGL2006-07404, founded by Ministerio de Educación y Ciencia (Spanish Government) and LE020A07, founded by Junta de Castilla y León. Adrián Melón-Nava was supported by the FPU program from the Spanish Ministerio de Universidades (FPU20/01220). Electrical Resistivity Tomography was performed by Geozone company (http://www.geozone.es/) in a very difficult conditions. Sergio Alberto Peña contributed to obtain drone images and detailed ortophotos generation from them. Two anonymous reviewers contributed to improve the initial version of the manuscript.

Appendix A. Supplementary material

Supplementary data to this article can be found online at https://doi.org/10.1016/j.catena.2022.106110.

References

Alonso-González, E., Ignacio López-Moreno, J., Gascoin, S., García-Valdecasas Ojeda, M., Sanmiguel-Vallelado, A., Navarro-Serrano, F., Revuelto, J., Ceballos, A., Esteban-Parra, M.J., Essery, R., 2018. Daily gridded datasets of snow depth and snow water equivalent for the Iberian Peninsula from 1980 to 2014. Syst. Sci. Data. https://doi.org/10.5194/essd-10-303-2018.

Alonso-González, E., López-Moreno, J.I., Navarro-Serrano, F., Sanmiguel-Vallelado, A., Aznárez-Balta, M., Revuelto, J., Ceballos, A., 2020. Snowpack sensitivity to temperature, precipitation, and solar radiation variability over an elevational gradient in the Iberian mountains. Atmos. Res. 243, 104973. https://doi.org/10.1016/j.atmosres.2020.104973.

Apaloo, J., Brenning, A., Bodin, X., 2012. Interactions between Seasonal Snow Cover, Ground Surface Temperature and Topography (Andes of Santiago. Chile 23 (4), 277–291. https://doi.org/10.1002/ppp.1753.

Biskaborn, B.K., Smith, S.L., Noetzli, J., Matthes, H., Vieira, G., Streletskiy, D.A., Schoeneich, P., Romanovsky, V.E., Lewkowicz, A.G., Abramov, A., Allard, M., Boike, J., Cable, W.L., Christiansen, H.H., Delaloye, R., Diekmann, B., Drozdov, D., Etzelmüller, B., Grosse, G., Guglielmin, M., Ingeman-Nielsen, T., Isaksen, K., Ishikawa, M., Johansson, M., Johannsson, H., Joo, A., Kaverin, D., Kholodov, A., Konstantinov, P., Kröger, T., Lambiel, C., Lanckman, J.-P., Luo, D., Malkova, G., Meiklejohn, I., Moskalenko, N., Oliva, M., Phillips, M., Ramos, M., Sannel, A.B.K., Sergeev, D., Seybold, C., Skryabin, P., Vasiliev, A., Wu, Q., Yoshikawa, K., Zheleznyak, M., Lantuit, H., 2019. Permafrost is warming at a global scale. Nat Commun 10 (1). https://doi.org/10.1038/s41467-018-08240-4.

Bodin, X., Thibert, E., Fabre, D., Ribolini, A., Schoeneich, P., Francou, B., Reynaud, L., Fort, M., 2009. Two decades of responses (1986–2006) to climate by the laurichard rock glacier. Permafr. Periglac. Process. 20 (4), 331–344. https://doi.org/10.1002/ppp.665.

Brenning, A., Gruber, S., Hoelzle, M., 2005. Sampling and statistical analyses of BTS measurements. Permafr. Periglac. Process. 16 (4), 383–393. https://doi.org/10.1002/ppp.541.

Colucci, R.R., Forte, E., Žebre, M., Maset, E., Zanettini, C., Guglielmin, M., 2019. Is that a relict rock glacier? Geomorphology 330, 177–189. https://doi.org/10.1016/j.geomorph.2019.02.002.

Davesne, G., Fortier, D., Domine, F., Gray, J.T., 2017. Wind-driven snow conditions control the occurrence of contemporary marginal mountain permafrost in the Chic-Choc Mountains, south-eastern Canada: A case study from Mont Jacques-Cartier. Cryosphere. https://doi.org/10.5194/tc-11-1351-2017.

Delaloye, R., Lambiel, C., 2005. Evidence of winter ascending air circulation throughout talus slopes and rock glaciers situated in the lower belt of alpine discontinuous permafrost (Swiss Alps). Norsk Geografisk Tidsskrift - Norwegian Journal of Geography 59 (2), 194–203. https://doi.org/10.1080/00291950510020673.

Delaloye, R., Reynard, E., Lambiel, C., Marescot, L., Monnet, R., 2003. Thermal anomaly in a cold scree slope (Creux du Van, Switzerland). Proc. Eighth Int. Conf, Permafrost, Zürich, Switzerland.

Duvillard, P.A., Revil, A., Qi, Y., Soueid Ahmed, A., Coperey, A., Ravanel, L., 2018. Three-Dimensional Electrical Conductivity and Induced Polarization Tomography of a Rock Glacier. J. Geophys. Res. Solid Earth. 123 (11), 9528–9554. https://doi.org/10.1029/2018JB015965.

Elder, K., Dozier, J., Michaelsen, J., 1991. Snow accumulation and distribution in an Alpine Watershed. Water Resour. Res. 27 (7), 1541–1552. https://doi.org/10.1029/91WR00506.

Emmert, A., Kneisel, C., 2017. Internal structure of two alpine rock glaciers investigated by quasi-3-D electrical resistivity imaging. Cryosphere 11 (2), 841–855. https://doi.org/10.5194/tc-11-841-2017.

Etzelmüller, B., 2013. Recent advances in mountain permafrost research. Permafr. Periglac. Process. 24 (2), 99–107. https://doi.org/10.1002/ppp.1772.

Evans, I.S., Cox, N.J., 2015. Size and shape of glacial cirques: comparative data in specific geomorphometry. Geomorphometry.

Fernandes, M., Palma, P., Lopes, L., Ruiz-Fernández, J., Pereira, P., Oliva, M., 2018. Spatial distribution and morphometry of permafrost-related landforms in the Central Pyrenees and associated paleoclimatic implications. Quat. Int. 470, 96–108. https://doi.org/10.1016/j.quaint.2017.08.071.

Ferreira, A., Vieira, G., Ramos, M., Nieuwendam, A., 2017. Ground temperature and permafrost distribution in Hurd Peninsula (Livingston Island. Catena 149, 560–571. https://doi.org/10.1016/j.catena.2016.08.027.

Frochoso, M., Castañón, J.C., 1996. El relieve heredado de la glaciación cuaternaria en el Macizo de Peña Prieta (Cordillera Cantábrica). Polígonos 6, 25–43. https://doi.org/10.18002/pol.v0i6.1069.

Gómez-Ortiz, A., Oliva, M., Salvador-Franch, F., Palacios, D., Tanarro, L.M., Sanjosé-Blasco, J.J., Salvà-Catarineu, M., 2019. Monitoring permafrost and periglacial processes in Sierra Nevada (Spain) from 2001 to 2016. Permafr. Periglac. Processes 30 (4), 278–291. https://doi.org/10.1002/ppp.2002.

Gómez-Ortiz, A., Salvà-Catarineu, M., Palacios, D., 2011. Caracterización térmica de la capa activa de un glaciar rocoso en medio periglaciar de alta montaña mediterránea: El ejemplo del Corral del Veleta (Sierra Nevada, España). Cuad. Investig. Geográfica 37 (2), 25–48. https://doi.org/10.18172/cig.1255.

Gómez-Villar, A., González-Gutiérrez, R.B., Redondo-Vega, J.M., Santos-González, J., 2011. Distribution of relict rock glaciers in the cantabrian mountains (León, Spain). Cuad. Investig. Geogr. 37, 49–80. https://doi.org/10.18172/cig.1256.

González-García, M., Serrano, E., Sanjosé-Blasco, J.J., González-Trueba, J.J., 2017. Surface dynamic of a protalus lobe in the temperate high mountain. Catena 149, 689–700. https://doi.org/10.1016/j.catena.2016.08.011.

Gruber, S., Haeberli, W., 2009. Permafrost Soils. In: Margesin, R. (Ed.), Soil Biology. Springer, Berlin, Heidelberg, pp. 33–44. https://doi.org/10.1007/978-3-540-69371-0_3.
Gubler, S., Fiddes, J., Keller, M., Gruber, S., 2011. Scale-dependent measurement and analysis of ground surface temperature variability in alpine terrain. Cryosphere 5 (2), 431–443. https://doi.org/10.5194/tc-5-431-201110.5194/tc-5-431-2011.
Haberkorn, A., Phillips, M., Kenner, R., Rhyner, H., Bavay, M., Galos, S.P., Hoelzle, M., 2015. Thermal Regime of Rock and its Relation to Snow Cover in Steep Alpine Rock Walls: Gemsstock. Geografiska Annaler: Series A, Physical Geography 97 (3), 579–597. https://doi.org/10.1111/geoa.12101.
Haeberli, W., 1975. Untersuchungen zur Verbreitung von Permafrost zwischen Flüelapass und Piz Grialetsch (Graubünden). Mitt Versuchsanst Wasserbau Hydrol Glaziologie Eidg Tech Hochsch Zurich.
Haeberli, W., Noetzli, J., Arenson, L., Delaloye, R., Gärtner-Roer, I., Gruber, S., Isaksen, K., Kneisel, C., Krautblatter, M., Phillips, M., 2011. Mountain permafrost: Development and challenges of a young research field. J. Glaciol. 56 (200), 1043–1058. https://doi.org/10.3189/002214311796406121.
Hanson, S., Hoelzle, M., 2004. The thermal regime of the active layer at the Murtèl rock glacier based on data from 2002. Permafr. Periglac. Process. 15 (3), 273–282. https://doi.org/10.1002/ppp.499.
Harris, C., Arenson, L.U., Christiansen, H.H., Etzelmüller, B., Frauenfelder, R., Gruber, S., Haeberli, W., Hauck, C., Hölzle, M., Humlum, O., Isaksen, K., Kääb, A., Kern-Lütschg, M.A., Lehning, M., Matsuoka, N., Murton, J.B., Nötzli, J., Phillips, M., Ross, N., Seppälä, M., Springman, S.M., Vonder Mühll, D., 2009. Permafrost and climate in Europe: Monitoring and modelling thermal, geomorphological and geotechnical responses. Earth-Science Rev 92 (3-4), 117–171. https://doi.org/10.1016/j.earscirev.2008.12.002.
Harris, S.A., Corte, A.E., 1992. Interactions and relations between mountain permafrost, glaciers, snow and water. Permafr. Periglac. Process. 3 (2), 103–110. https://doi.org/10.1002/ppp.3430030207.
Harris, S.A., Pedersen, D.E., 1998. Thermal regimes beneath coarse blocky materials. Permafr. Periglac. Process. https://doi.org/10.1002/(SICI)1099-1530(199804/06)9:2<107::AID-PPP277>3.0.CO;2-G.
He, S., Ohara, N., 2017. A New Formula for Estimating the Threshold Wind Speed for Snow Movement. J. Adv. Model. Earth Syst. 9 (7), 2514–2525. https://doi.org/10.1002/2017MS000982.
Hilbich, C., Marescot, L., Hauck, C., Loke, M.H., Mäusbacher, R., 2009. Applicability of electrical resistivity tomography monitoring to coarse blocky and ice-rich permafrost landforms. Permafr. Periglac. Process. 20 (3), 269–284. https://doi.org/10.1002/ppp.652.
Hoelzle, M., 1992. Permafrost occurrence from BTS measurements and climatic parameters in the eastern Swiss Alps. Permafr. Periglac. Process. 3 (2), 143–147. https://doi.org/10.1002/ppp.3430030212.
Hoelzle, M., Wegmann, M., Krummenacher, B., 1999. Miniature temperature dataloggers for mapping and monitoring of permafrost in high mountain areas: First experience from the Swiss Alps. Permafr. Periglac. Process. https://doi.org/10.1002/(SICI)1099-1530(199904/06)10:2<113::AID-PPP317>3.0.CO;2-A.
Hrbáček, F., Oliva, M., Fernández, J.-R., Kňažková, M., de Pablo, M.A., 2020. Modelling ground thermal regime in bordering (dis)continuous permafrost environments. Environ. Res. 181, 108901. https://doi.org/10.1016/j.envres.2019.108901.
Ishikawa, M., 2003. Thermal regimes at the snow-ground interface and their implications for permafrost investigation. Geomorphology 52 (1-2), 105–120. https://doi.org/10.1016/S0169-555X(02)00251-9.
Ishikawa, M., Hirakawa, K., 2000. Mountain permafrost distribution based on BTS measurements and DC resistivity soundings in the Daisetsu Mountains, Hokkaido, Japan. Permafr. Periglac. Process. https://doi.org/10.1002/1099-1530(200004/06)11:2<109::AID-PPP343>3.0.CO;2-O.
Julián, A., Chueca, J., 2007. Permafrost distribution from BTS measurements (Sierra de Telera, central Pyrenees, Spain): Assessing the importance of solar radiation in a mid-elevation shaded mountainous area. Permafr. Periglac. Process. 18 (2), 137–149. https://doi.org/10.1002/ppp.576.
Juliussen, H., Humlum, O., 2008. Thermal regime of openwork block fields on the mountains Elgåhogna and Sølen, central-eastern Norway. Permafr. Periglac. Process. https://doi.org/10.1002/ppp.607.
Kellerer-Pirklbauer, A., 2019. Long-term monitoring of sporadic permafrost at the eastern margin of the European Alps (Hochreichart. Permafr. Periglac. Process. 30 (4), 260–277. https://doi.org/10.1002/ppp.2021.
Kenner, R., Phillips, M., Hauck, C., Hilbich, C., Mulsow, C., Bühler, Y., Stoffel, A., Buchroithner, M., 2017. New insights on permafrost genesis and conservation in talus slopes based on observations at Flüelapass. Geomorphology 290, 101–113. https://doi.org/10.1016/j.geomorph.2017.04.011.
Kneisel, C., Hauck, C., Mühll, D.V., 2000. Permafrost below the Timberline confirmed and characterized by geoelectrical resistivity measurements, Bever Valley, eastern Swiss Alps. Permafr. Periglac. Process. https://doi.org/10.1002/1099-1530(200012)11:4<295::AID-PPP353>3.0.CO;2-L.
Lambiel, C., Pieracci, K., 2008. Permafrost distribution in talus slopes located within the alpine periglacial belt, Swiss alps. Permafr. Periglac. Process. https://doi.org/10.1002/ppp.624.
Lewkowicz, A.G., Etzelmüller, B., Smith, S.L., 2011. Characteristics of discontinuous permafrost based on ground temperature measurements and electrical resistivity tomography. Permafr. Periglac. Process. 22 (4), 320–342. https://doi.org/10.1002/ppp.703.
Ling, F., Zhang, T., 2003. Impact of the timing and duration of seasonal snow cover on the active layer and permafrost in the Alaskan Arctic. Permafr. Periglac. Process. 14 (2), 141–150. https://doi.org/10.1002/ppp.445.
López-Moreno, J.I., Soubeyroux, J.M., Gascoin, S., Alonso-Gonzalez, E., Durán-Gómez, N., Lafaysse, M., Vernay, M., Carmagnola, C., Morin, S., 2020. Long-term trends (1958–2017) in snow cover duration and depth in the Pyrenees. Int. J. Climatol. 40 (14), 6122–6136. https://doi.org/10.1002/joc.6571.
Luetschg, M., Lehning, M., Haeberli, W., 2008. A sensitivity study of factors influencing warm/thin permafrost in the Swiss Alps. J. Glaciol. 54 (187), 696–704. https://doi.org/10.3189/002214308786570881.
Lugon, R., Delaloye, R., Serrano, E., Reynard, E., Lambiel, C., González-Trueba, J.J., 2004. Permafrost and Little Ice Age glacier relationships, posets massif, central Pyrenees. Permafr. Periglac. Process. 15 (3), 207–220. https://doi.org/10.1002/ppp.494.
Magnin, F., Westermann, S., Pogliotti, P., Ravanel, L., Deline, P., Malet, E., 2017. Snow control on active layer thickness in steep alpine rock walls (Aiguille du Midi, 3842 m a.s.l., Mont Blanc massif). Catena 149, 648–662. https://doi.org/10.1016/j.catena.2016.06.006.
Marmy, A., Salzmann, N., Scherler, M., Hauck, C., 2013. Permafrost model sensitivity to seasonal climatic changes and extreme events in mountainous regions. Environ. Res. Lett. 8 (3), 035048. https://doi.org/10.1088/1748-9326/8/3/035048.
Martín-González, F., Heredia, N., 2011. Geometry, structures and evolution of the western termination of the Alpine-Pyrenean Orogen reliefs (NW Iberian Peninsula). J. Iber. Geol. 37, 103–120. https://doi.org/10.5209/rev_JIGE.2011.v37.n2.1.
Martínez-Catalán, J.R., Aller, J., Alonso, J.L., Bastida, F., 2009. The Iberian Variscan orogen. In: García-Cortés, A., Villar, J.A., Suárez-Valngrande, Salvador González, C.I. Spanish geological frameworks and geosites. Instituto Geológico y Minero de España, Madrid, 13-30. https://www.igme.es/patrimonio/GEOSITES/Chapter_01_SGFG.pdf.
Mollaret, C., Hilbich, C., Pellet, C., Flores-Orozco, A., Delaloye, R., Hauck, C., 2019. Mountain permafrost degradation documented through a network of permanent electrical resistivity tomography sites. Cryosphere 13 (10), 2557–2578. https://doi.org/10.5194/tc-13-2557-201910.5194/tc-13-2557-2019-supplement.
Morard, S., Delaloye, R., Lambiel, C., 2010. Pluriannual thermal behavior of low elevation cold talus slopes in western Switzerland. Geogr. Helv. https://doi.org/10.5194/gh-65-124-2010.
Mott, R., Schirmer, M., Bavay, M., Grünewald, T., Lehning, M., 2010. Understanding snow-transport processes shaping the mountain snow-cover. Cryosphere 4 (4), 545–559. https://doi.org/10.5194/tc-4-545-2010.
Navarro-Serrano, F., López-Moreno, J.I., 2017. Spatio-temporal analysis of snowfall events in the spanish Pyrenees and their relationship to atmospheric circulation. Cuad. Investig. Geográfica 43 (1), 233–254. https://doi.org/10.18172/cig.3042.
Ohmura, A., 2001. Physical basis for the temperature-based melt-index method. J. Appl. Meteorol. https://doi.org/10.1175/1520-0450(2001)040<0753:PBFTTB>2.0.CO;2.
Oliva, M., Žebre, M., Guglielmin, M., Hughes, P.D., Çiner, A., Vieira, G., Bodin, X., Andrés, N., Colucci, R.R., García-Hernández, C., Mora, C., Nofre, J., Palacios, D., Pérez-Alberti, A., Ribolini, A., Ruiz-Fernández, J., Sarıkaya, M.A., Serrano, E., Urdea, P., Valcárcel, M., Woodward, J.C., Yıldırım, C., 2018. Permafrost conditions in the Mediterranean region since the Last Glaciation. Earth-Science Rev 185, 397–436. https://doi.org/10.1016/j.earscirev.2018.06.018.
Onaca, A., Ardelean, A.C., Urdea, P., Ardelean, F., Sîrbu, F., 2015. Detection of mountain permafrost by combining conventional geophysical methods and thermal monitoring in the Retezat Mountains. Cold Regions Science and Technology 119, 111–123. https://doi.org/10.1016/j.coldregions.2015.08.001.
Onaca, A., Ardelean, F., Ardelean, A., Magori, B., Sîrbu, F., Voiculescu, M., Gachev, E., 2020. Assessment of permafrost conditions in the highest mountains of the Balkan Peninsula. Catena 185, 104288. https://doi.org/10.1016/j.catena.2019.104288.
Ortega-Villazán, M.T., Morales-Rodríguez, C.G., 2015. El clima de la Cordillera Cantábrica castellano-leonesa: diversidad, contrastes y cambios. Investig. Geográficas. https://doi.org/10.14198/ingeo2015.63.04.
Outcalt, S.I., Nelson, F.E., Hinkel, K.M., 1990. The zero-curtain effect: Heat and mass transfer across an isothermal region in freezing soil. Water Resour. Res. 26 (7), 1509–1516. https://doi.org/10.1029/WR026i007p01509.
Pellitero, R., 2014. Geomorphology and geomorphological landscapes of Fuentes Carrionas. J. Maps 10 (2), 313–323. https://doi.org/10.1080/17445647.2013.867822.
Pellitero, R., Serrano, E., González Trueba, J.J., 2011. Rock glaciers in the central cantabrian mountains: Palaeoenvironmental indicators. Cuad. Investig. Geogr. 37, 119–144. https://doi.org/10.18172/cig.1259.
Pellitero, R., 2022. The glaciers of the Montaña Palentina. Iberia, Land of Glaciers. Elsevier, pp. 179–199. https://doi.org/10.1016/B978-0-12-821941-6.00009-8.
Pellitero, R., Fernández-Fernández, J.M., Campos, N., Serrano, E., Pisabarro, A., 2019. Late Pleistocene climate of the northern Iberian Peninsula: New insights from palaeoglaciers at Fuentes Carrionas (Cantabrian Mountains). J. Quat. Sci. 34 (4-5), 342–354. https://doi.org/10.1002/jqs.3106.
Pisabarro, A., 2020. Snow cover as a morphogenic agent determining ground climate, landforms and runoff in the valdecebollas massif, cantabrian mountains. Geogr. Res. Lett. https://doi.org/10.18172/cig.3823.
Pisabarro Pérez, A., Serrano Cañadas, E., González Trueba, J.J., 2015. Régimen térmico de suelos del macizo Central de picos de Europa (España). Pirineos 170 (0), e010. https://doi.org/10.3989/pirineos.2015.v17010.3989/Pirineos.2015.170003.
Pisabarro, A., Pellitero, R., Serrano, E., Gómez-Lende, M., González-Trueba, J.J., 2017. Ground temperatures, landforms and processes in an Atlantic mountain. Catena 149, 623–636. https://doi.org/10.1016/j.catena.2016.07.051.
Popescu, R., Vespremeanu-Stroe, A., Onaca, A., Vasile, M., Cruceru, N., Pop, O., 2017. Low-altitude permafrost research in an overcooled talus slope–rock glacier system in the Romanian Carpathians (Detunata Goală Apuseni Mountains). Geomorphology 295, 840–854. https://doi.org/10.1016/j.geomorph.2017.07.029.
Prado, C., 1852. Note sur les blocs erratiques de la chaine cantabrique. Bull. la Soc. Géologique Fr. 9, 171–175.

Raska, P., Kirchner, K., Raska, M., 2011. Winter microclimatic regime of low-altitude scree slopes and its relation to topography: Case study from the Ceske Stredohori Mts. (N Czech Republic). Geogr. Fis. e Din. Quat. https://doi.org/10.4461/GFDQ.2011.34.21.

Redondo Vega, J.M., Gómez Villar, A., González Gutiérrez, R.B., Santos González, J., 2011. Los glaciares rocosos de la Cordillera Cantábrica. Universidad de León, León.

Redondo-Vega, J.M., Santos-González, J., 2013. Dinámica y morfología glaciar en el valle de Cardaño, Palencia (Cordillera Cantábrica). Boletín de la Asociación de Geógrafos Españoles 62, 173–188. https://doi.org/10.21138/bage.1574.

Ribolini, A., Guglielmin, M., Fabre, D., Bodin, X., Marchisio, M., Sartini, S., Spagnolo, M., Schoeneich, P., 2010. The internal structure of rock glaciers and recently deglaciated slopes as revealed by geoelectrical tomography: insights on permafrost and recent glacial evolution in the Central and Western Alps (Italy-France). Quat. Sci. Rev. 29 (3-4), 507–521. https://doi.org/10.1016/j.quascirev.2009.10.008.

Rödder, T., Kneisel, C., 2012. Influence of snow cover and grain size on the ground thermal regime in the discontinuous permafrost zone. Geomorphology 175-176, 176–189. https://doi.org/10.1016/j.geomorph.2012.07.008.

Rodríguez-Fernández, L.R., Heredia, N., Navarro, D., Martínez-García, E., Marquínez, J., 1994. Mapa Geológico de España E. 1:50.000, Hoja Nº 81, Potes. Instituto Geológico y Minero de España.

Ruiz-Fernández, J., Oliva, M., Hrbáček, F., Vieira, G., García-Hernández, C., 2017. Soil temperatures in an Atlantic high mountain environment: The Forcadona buried ice patch (Picos de Europa. Catena 149, 637–647. https://doi.org/10.1016/j.catena.2016.06.037.

Santos-González, J., González-Gutiérrez, R., Gómez-Villar, A., Redondo-Vega, J., 2009. Ground thermal regime in the vicinity of relict rock glaciers (Cantabrian Mountains, NW Spain). Finisterra 44. https://doi.org/10.18055/finis1375.

Santos-González, J., Redondo-Vega, J.M., García-de Celis, A., González-Gutiérrez, R.B., Gómez-Villar, A., 2022. The glaciers of the Leonese Cantabrian Mountains. Iberia, Land of Glaciers. Elsevier, pp. 289–314. https://doi.org/10.1016/B978-0-12-821941-6.00014-1.

Santos-González, J., Redondo-Vega, J.M., González-Gutiérrez, R.B., Gómez-Villar, A., 2013. Applying the AABR method to reconstruct equilibrium-line altitudes from the last glacial maximum in the Cantabrian Mountains (SW Europe). Palaeogeogr. Palaeoclimatol. Palaeoecol. 387, 185–199. https://doi.org/10.1016/j.palaeo.2013.07.025.

Sawada, Y., Ishikawa, M., Ono, Y., 2003. Thermal regime of sporadic permafrost in a block slope on Mt. Geomorphology 52 (1-2), 121–130. https://doi.org/10.1016/S0169-555X(02)00252-0.

Scapozza, C., Lambiel, C., Baron, L., Marescot, L., Reynard, E., 2011. Internal structure and permafrost distribution in two alpine periglacial talus slopes. Geomorphology 132 (3-4), 208–221. https://doi.org/10.1016/j.geomorph.2011.05.010.

Schmid, M.-O., Gubler, S., Fiddes, J., Gruber, S., 2012. Inferring snowpack ripening and melt-out from distributed measurements of near-surface ground temperatures. Cryosphere 6 (5), 1127–1139. https://doi.org/10.5194/tc-6-1127-201210.5194/tc-6-1127-2012-supplement.

Schneider, S., Hoelzle, M., Hauck, C., 2012. Influence of surface and subsurface heterogeneity on observed borehole temperatures at a mountain permafrost site in the Upper Engadine, Swiss Alps. Cryosphere. https://doi.org/10.5194/tc-6-517-2012.

Senese, A., Maugeri, M., Vuillermoz, E., Smiraglia, C., Diolaiuti, G., 2014. Using daily air temperature thresholds to evaluate snow melting occurrence and amount on Alpine glaciers by T-index models: The case study of the Forni Glacier (Italy). Cryosphere. https://doi.org/10.5194/tc-8-1921-2014.

Serrano, E., González-Trueba, J., 2004. Morfodinámica periglaciar en el Grupo Peña Vieja (macizo central de los Picos de Europa - Cantabria -). Cuaternario y Geomorfol. 18 (3), 73–88. https://doi.org/10.18172/cig.3042.

Serrano, E., González-Trueba, J.J., Pellitero, R., González-García, M., Gómez-Lende, M., 2013. Quaternary glacial evolution in the Central Cantabrian Mountains (Northern Spain). Geomorphology 196, 65–82. https://doi.org/10.1016/j.geomorph.2012.05.001.

Serrano, E., Gómez-Lende, M., Pellitero, R., González Trueba, J.J., 2015. Deglaciation in the Cantabrian Mountains: pattern and evolution. Cuad. Investig. Geográfica 41, 389. https://doi.org/10.18172/cig.2716.

Serrano, E., Sanjosé-Blasco, J.J., Gómez-Lende, M., López-Moreno, J.I., Pisabarro, A., Martínez-Fernández, A., 2019. Periglacial environments and frozen ground in the central Pyrenean high mountain area: Ground thermal regime and distribution of landforms and processes. Permafr. Periglac. Process. 30 (4), 292–309. https://doi.org/10.1002/ppp.2032.

Serrano, E., López-Moreno, J.I., Gómez-Lende, M., Pisabarro, A., Martín-Moreno, R., Rico, I., Alonso-González, E., 2020. Frozen ground and periglacial processes relationship in temperate high mountains: a case study at Monte Perdido-Tucarroya area (The Pyrenees, Spain). J. Mt. Sci. 17 (5), 1013–1031. https://doi.org/10.1007/s11629-019-5614-5.

Staub, B., Delaloye, R., 2017. Using Near-Surface Ground Temperature Data to Derive Snow Insulation and Melt Indices for Mountain Permafrost Applications. Permafr. Periglac. Process. 28 (1), 237–248. https://doi.org/10.1002/ppp.1890.

Staub, B., Marmy, A., Hauck, C., Hilbich, C., Delaloye, R., 2015. Ground temperature variations in a talus slope influenced by permafrost: A comparison of field observations and model simulations. Geogr. Helv. https://doi.org/10.5194/gh-70-45-2015.

Stiegler, C., Rode, M., Sass, O., Otto, J.C., 2014. An Undercooled Scree Slope Detected by Geophysical Investigations in Sporadic Permafrost below 1000 M ASL, Central Austria. Permafr. Periglac. Process. https://doi.org/10.1002/ppp.1813.

Strand, S.M., 2016. Ground temperature response to winter warm events in Svalbard. A periglacial landform comparison. University of Oslo.

Streletskiy, D.A., Sherstiukov, A.B., Frauenfeld, O.W., Nelson, F.E., 2015. Changes in the 1963–2013 shallow ground thermal regime in Russian permafrost regions. Environ. Res. Lett. 10 (12), 125005. https://doi.org/10.1088/1748-9326/10/12/125005.

Sysolyatin, R., Serikov, S., Zheleznyak, M., Tikhonravova, Y., Skachkov, Y., Zhizhin, V., Rojina, M., 2020. Temperature monitoring from 2012 to 2019 in central part of Suntar-Khayat Ridge. J. Mt. Sci. 17 (10), 2321–2338. https://doi.org/10.1007/s11629-020-6175-3.

Thorn, C.E., Schlyter, J.P.L., Darmody, R.G., Dixon, J.C., 1999. Statistical relationships between daily and monthly air and shallow-ground temperatures in Karkevagge, Swedish Lapland. Permafr. Periglac. Process. https://doi.org/10.1002/(SICI)1099-1530(199910/12)10:4<317::AID-PPP329>3.0.CO;2-S.

Throop, J., Lewkowicz, A.G., Smith, S.L., 2012. Climate and ground temperature relations at sites across the continuous and discontinuous permafrost zones, northern Canada. Can. J. Earth Sci. https://doi.org/10.1139/E11-075.

Vieira, G.T., Mora, C., Ramos, M., 2003. Ground temperature regimes and geomorphological implications in a Mediterranean mountain (Serra da Estrela, Portugal). Geomorphology 52 (1-2), 57–72. https://doi.org/10.1016/S0169-555X(02)00248-9.

Wakonigg, H., 1996. Unterkühlte Schutthalden. Beiträge zur Permafrostforschung in Österreich. In: Arb. aus dem Inst. für Geogr, 33. der Karl-Franzens-Universität Graz, pp. 209–223.

Westermann, S., Boike, J., Langer, M., Schuler, T.V., Etzelmüller, B., 2011. Modeling the impact of wintertime rain events on the thermal regime of permafrost. Cryosphere 5 (4), 945–959. https://doi.org/10.5194/tc-5-945-2011.

Wicky, J., Hauck, C., 2020. Air Convection in the Active Layer of Rock Glaciers. Front. Earth Sci. https://doi.org/10.3389/feart.2020.00335.

Williams, G., Gold, L., 1976. CBD-180 Ground Temperatures. National Research Council Canada 100.

Yu, W., Lai, Y., Zhang, X., Zhang, S., Xiao, J., 2004. Laboratory investigation on cooling effect of coarse rock layer and fine rock layer in permafrost regions. Cold Reg. Sci. Technol. 38 (1), 31–42. https://doi.org/10.1016/S0165-232X(03)00061-2.

Zacharda, M., Gude, M., Růžička, V., 2007. Thermal regime of three low elevation scree slopes in central Europe. Permafr. Periglac. Process. 18 (3), 301–308. https://doi.org/10.1002/ppp.598.

Zhang, T., 2005. Influence of the seasonal snow cover on the ground thermal regime: An overview. Rev. Geophys. 43 (4) https://doi.org/10.1029/2004RG000157.

Zhao, J.-y., Chen, J.i., Wu, Q.-B., Hou, X., 2018. Snow cover influences the thermal regime of active layer in Urumqi River Source. J. Mt. Sci. 15 (12), 2622–2636. https://doi.org/10.1007/s11629-018-4856-y.

Zhou, J., Kinzelbach, W., Cheng, G., Zhang, W., He, X., Ye, B., 2013. Monitoring and modeling the influence of snow pack and organic soil on a permafrost active layer, qinghai-tibetan plateau of china. Cold Reg. Sci. Technol. 90-91, 38–52. https://doi.org/10.1016/j.coldregions.2013.03.003.

Zingg, T., 1951. Beziehung zwischen Temperatur und Schmelzwasser und ihre Bedeutung für Niederschlags- und Abflussfragen. IUGG General Assembly of Bruxelles, IAHS Publications 33, 266–299.